Award Number: W81XWH-12-1-0251

TITLE: Therapeutic Role of Bmi-1 Inhibitors in Eliminating Prostate Tumor Stem Cells

PRINCIPAL INVESTIGATOR: Isaac Kim, MD, PhD

CONTRACTING ORGANIZATION: Rutgers, The State University of New jersey- RBHS-CINJ
                                                    New Brunswick, NJ 08901

REPORT DATE: October 2015

TYPE OF REPORT: Annual

PREPARED FOR: U.S. Army Medical Research and Materiel Command
                            Fort Detrick, Maryland 21702-5012

DISTRIBUTION STATEMENT: Approved for Public Release;
                                            Distribution Unlimited

REPORT DOCUMENTATION PAGE

Form Approved
OMB No. 0704-0188

Public reporting burden for this collection of information is estimated to average 1 hour per response, including the time for reviewing instructions, searching existing data sources, gathering and maintaining the data needed, and completing and reviewing this collection of information. Send comments regarding this burden estimate or any other aspect of this collection of information, including suggestions for reducing this burden to Department of Defense, Washington Headquarters Services, Directorate for Information Operations and Reports (0704-0188), 1215 Jefferson Davis Highway, Suite 1204, Arlington, VA 22202-4302. Respondents should be aware that notwithstanding any other provision of law, no person shall be subject to any penalty for failing to comply with a collection of information if it does not display a currently valid OMB control number. **PLEASE DO NOT RETURN YOUR FORM TO THE ABOVE ADDRESS.**

1. REPORT DATE	2. REPORT TYPE	3. DATES COVERED
October 2015	Annual	30 Sep 2014 - 29 Sep 2015

4. TITLE AND SUBTITLE

Therapeutic Role of Bmi-1 Inhibitors in Eliminating Prostate Tumor Stem Cells

5a. CONTRACT NUMBER
W81XWH-12-1-0251

5b. GRANT NUMBER:

5c. PROGRAM ELEMENT NUMBER

6. AUTHOR(S)

Isaac Kim, MD, PhD (Partnering PI),
Joseph Bertino, MD (Partnering PI),
Hatem E. Sabaawy, MD, PhD (Initiating PI).

E-Mail: kimiy@cinj.rutgers.edu

5d. PROJECT NUMBER

5e. TASK NUMBER

5f. WORK UNIT NUMBER

7. PERFORMING ORGANIZATION NAME(S) AND ADDRESS(ES)

UMDNJ-Robert Wood Johnson Medical School (name and address on the contract)
675 Hoes LN, Piscataway NJ 08854-5627

Rutgers, The State University of New jersey- RBHS-CINJ (current name)
3 Rutgers Plaza, ASB III-2nd floor, New Brunswick, NJ 08901-8559

8. PERFORMING ORGANIZATION REPORT NUMBER

9. SPONSORING / MONITORING AGENCY NAME(S) AND ADDRESS(ES)

U.S. Army Medical Research and Materiel Command
Fort Detrick, Maryland 21702-5012

10. SPONSOR/MONITOR'S ACRONYM(S)

11. SPONSOR/MONITOR'S REPORT NUMBER(S)

12. DISTRIBUTION / AVAILABILITY STATEMENT
Approved for Public Release; Distribution Unlimited

13. SUPPLEMENTARY NOTES

14. ABSTRACT

Current prostate cancer (PCa) management calls for identifying novel and more effective therapeutic approaches that could target therapy resistant self-renewing prostate tumor-initiating cells (TICs). Our focus is on BMI-1 (B-cell-specific MMLV insertion site-1), a protein that regulates stem cell self-renewal. During the first two years of this award and in collaboration with the initiating and other partnering PIs, we have developed and optimized a time-of-adherence assay to identify TICs that we demonstrated to have $CD49b^{hi}CD29^{hi}CD44^{hi}$ cell phenotype. This year, we examined the first known translational inhibitors of BMI-1; C-209 to target prostate TICs alone and in combination with taxotere, the standard of care. Employment of this specific BMI-1 inhibitor on patient-derived cells significantly decreased spheroid formation *in vitro* and prevented tumor initiation *in vivo* in mice (Bertino Lab), thereby diminishing the frequency of TICs from a large number of patients' tissues. Furthermore, C-209 induced cell senescence, G1 cell cycle arrest, and reduced intratumor BMI-1 levels, while displaying antitumor activity in mouse xenografts did not exert toxic effects on normal tissues. BMI-1 targeted therapy when combined with taxotere resulted in further antitumor activities. Therefore, we have accomplished our third year's goal to demonstrate the beneficial effects of targeting prostate TICs *in vivo* in mice in this synergistic award between three laboratories (Sabaawy, Bertino, and Kim) to develop a therapeutic strategy for BMI-1 inhibitors in prostate cancer.

15. SUBJECT TERMS

16. SECURITY CLASSIFICATION OF:			17. LIMITATION OF ABSTRACT	18. NUMBER OF PAGES	19a. NAME OF RESPONSIBLE PERSON USAMRMC
a. REPORT	**b. ABSTRACT**	**c. THIS PAGE**	UU	88	**19b. TELEPHONE NUMBER** *(include area code)*
U	U	U			

CONTENTS

Preprint of Bansal et al., *Cell Res.*, submitted. (Manuscript, supplemental material and Editorial and peer review comments).

A. INTRODUCTION

The approved statement of work (SOW) described synergistic efforts of three laboratories; my laboratory-PI (Isaac Kim, MD, PhD; contract #W81XWH-12-1-0251), that of the initiating PI (Hatem Sabaawy, MD, PhD; contract #W81XWH-12-1-0249); and partnering-PI (Joseph Bertino, MD; contract #W81XWH-12-1-0250) to develop small molecule inhibitors against BMI-1 (B-cell-specific MMLV insertion site-1) in prostate cancer. Prostate tumor-initiating cells (TICs) have intrinsic resistance to current therapies. BMI-1 regulates stem cell self-renewal, and is over-expressed in TICs. Our group developed a combined immunophenotypic and time-of-adherence assay to identify human prostate TICs with increased BMI-1 expression. Our goal is to identify and subsequently develop a new class of bioavailable small molecules that inhibit tumor growth by selectively reducing BMI-1 production.

The following tasks from **the approved SOW** were performed to achieve the goal of defining the strategy for use of effective BMI-1 inhibitors in future trials:

Task #1. My laboratory has completed this task of evaluation of the expression of markers of TICs such as BMI-1 and CD44 and correlation with prostate cancer markers in prostate cancer patients using IHC. We demonstrated the correlation of BMI-1 and CD44 expression in TICs in the accomplished tasks sections, and correlation of TICs expression to PCa markers AMACR[1] and Erg in the published manuscript[2] and additional data in the newly submitted manuscript (Bansal et al., *Cell Res.* manuscript in revision that is attached in the Appendix).

Task #2. Completed by Bertino Lab.

Task #3. Completed by Sabaawy Lab.

Task #4. Completed by both Sabaawy and Bertino Labs.

From the above experiments performed in the third year of the project, I isolated prostatectomy tissues and primary PCa cells were isolated in my laboratory. These cells were utilized by the collaborating labs and we have then determined that C-209 is the BMI-1 inhibitor that was successfully used for *in vivo* studies in zebrafish (Sabaawy Lab), and similar conclusions were achieved from mouse xenograft studies (Bertino Lab), therefore suggesting that this compound may be further pursued for PCa therapy. We have published one manuscript[2] from the studies of the first year and generated more data for additional manuscripts on the development and characterization of the mechanism of action of the BMI-1 inhibitor that will be completed during the extension year of the project.

B. BODY

Treatment of advanced prostate cancer (PCa) and castration resistant PCa (CRPC) have been challenging with limited success[3]. Newly approved therapies only marginally extend median survival by ~3 months[4,5], and resistance to these treatments are emerging. There is a dire need for therapies that are safe, efficacious, and cost-effective for treating CRPC, and can be used in early disease to prevent metastasis.

A fractions of PCa cells acquire and/or retain tumor initiation and self-renewal potentials, therefore are termed TICs[6,7]. We have identified prostate TICs from primary tissues that are collagen-adherent $\alpha2\beta1^{hi}$/CD44^{hi} cells[2]. Recent experimental and clinical studies have identified BMI-1 as a member of the polycomb family of chromatin remodeling complexes that act as transcriptional repressors for epigenetic chromatin modification. BMI-1 encodes a zinc finger protein that forms a key rate-limiting regulatory component of the polycomb repressor complex (PRC1) regulating cellular transcription. PRC1 enzymatic activities include DNA methylation of CpG islands and global mono-ubiquitination of histone 2A. Our data demonstrate that upregulated BMI-1 levels correlate with advanced PCa based on the scores derived from histopathology sections (Table 1). PCa TICs can self-renew and also generate non-TIC progeny[6]. Prostate TICs survive treatment due to their intrinsic resistance to current therapies[8,9]. BMI-1 is a central player in PCa progression as it controls growth signals[10-15], regulates oncogenic microRNAs[16], and induces metastasis markers [17]. BMI-1 is overexpressed at levels much higher in cancer cells vs. normal cells, and contributes to therapy resistance, in particular in advanced and/or metastatic PCa[10,18,19]. Importantly, the strongest BMI-1 expression is observed in tissues[20,21], and plasma[22-25] of highly aggressive tumors undergoing metastasis. Notably, BMI-1 protein levels in serum of PCa patients correlate with increased serum PSA[26]. Therefore, BMI-1 is an excellent biomarker for advanced PCa, and targeting BMI-1 is a compelling therapeutic approach.

Knockdown of BMI-1 inhibits cell proliferation and results in growth arrest[11]; whereas its overexpression promotes anchorage independent growth and cell invasion[12]. With recent sequencing of pancreatic and kidney cancers[27,28] and determination of mutational landscape of PCa[29], an unexpected intratumor heterogeneity was revealed. A common feature of these heterogeneous clones is self-renewal, a feature that can be effectively targeted by inhibiting BMI-1.

We identified primary PCa adherent $\alpha2\beta1^{hi}$/CD44^{hi} TICs in mouse and zebrafish xenografts[2] that overexpress BMI-1. TICs are comprised of heterogeneous subpopulations with multiple phenotypes[30]. Prostate TICs and invasive cells are enriched for CD44[31], suggesting an intriguing mechanism of initiating PCa invasion though basement membrane degrading activity of CD44^{hi} TICs. We demonstrate that BMI-1 inhibitors target these senescence targets. In summary, BMI-1 is a critical target in PCa and developing BMI-1 inhibitors will provide novel and effective therapy for PCa treatment.

C. ACCOMPLISHED TASKS

Task1. Evaluation of BMI-1 expression in PCa. BMI-1 is a potential target for human prostate TICs. We examined whether BMI-1 is upregulated in prostate cancer cells from an additional 24 patients this year, and whether it is coexpressed with the putative prostate TIC marker CD44 in primary prostate cancer tissues. To evaluate the clinical relevance of BMI-1 activation, we previously conducted BMI-1 and *CD44* expression analyses on FFPE human PCa by IHC. Clinical tissues were classified according to postoperative Gleason score or clinical stage (TNM system). Histological categories divided tumors with Gleason scores, whereas clinical stage groups were defined as prostate-confined disease (pT2) and disease with extraprostatic extension (pT3). First, PCa regions were identified with the granular cytoplasmic staining of AMACR[1] and ERG overexpression when TEMPRSS-ERG fusion was detected [2]. Sequential sections were then examined for expression of CD44 (progenitor isoform) and BMI-1. Early-stage adenocarcinomas showed upregulated BMI-1 and CD44 coexpression, as compared to normal margins.

The PI is a Surgical Oncologist specialized in robotic prostatectomy. After performing these surgeries, my laboratory was involved in this task of collecting TICs from these prostatectomies. On the basis of rapid adhesion on collagen, PCa cells were plated on a collagen-I dish for 5 min (5'=rapidly adherent) (3-5% of cells) were enriched for TICs by sorting the $\alpha_2\beta_1^{hi}$/CD44^{hi} cells. The sorted adherent cells upregulated CD133 (From 0.01% to ~3%), and this fraction showed superior ability to form tumors in mice[2]. The $\alpha2\beta1^{hi}$/CD44^{hi} cells have significantly higher colony forming efficiency, increased migration, and increased invasion abilities vs. $\alpha2\beta1^{low}$/CD44^{low} cells[2]. The ability of the $\alpha2\beta1^{hi}$/CD44^{hi} TICs to self-renew was tested in serial spheroid assays. Disaggregated primary spheroids from $\alpha2\beta1^{hi}$/CD44^{hi} cells reformed spheroids in 2^{ry} and 3^{ry} assays, whereas those from $\alpha2\beta1^{low}$/CD44^{low} cells formed only cell clusters in 2^{ry} assays, reflecting their limited stemness[2]. Thus, adherent $\alpha2\beta1^{hi}$/CD44^{hi} cells are more tumorigenic *in vitro*, and in mice, therefore fulfilled the criteria of TICs. We show in IHC on TMA and from primary PCa tissues that BMI-1 overexpression correlates with advanced disease, further confirming that BMI-1 is a TIC target.

These data from TMA were also seen in tissues from 24 patients who were recruited to this study (Table 1), are consistent with previous reports[10,18,19,26], and suggest that PCa patients would benefit from BMI-1-targeted therapies.

1^{ry} Prostate cancer	Age	Type	Grade	pTNM	Gleason	BMI-1 expression by IHC H-score
15728	62	Adc	3	pT2c	3 + 3	120
17148	52	Adc	3	pT2c	3 + 3	150
17761	57	Adc	3	pT2c	3 + 3	ND
19803	55	Adc	3	pT2c	3 + 3	70
24126	53	Adc	4	pT3a	3 + 3	190
40181	60	Adc	4	pT3a	3 + 4	ND
25185	67	Adc	3	pT2c	3 + 3	200
25315	66	Adc	4	pT3a	3 + 4	150
26136	67	Adc	3	pT3b	4 + 5	220
25854	55	Adc	4	pT3b	4 + 5	190
28838	65	Adc	4	pT3b	4 + 4	160
28864	68	Adc	3	pT3b	3 + 4	210
28869	67	Adc	4	pT2c	4 + 4	200
29032	68	Adc	4	pT3b	4 + 5	210
29084	58	Adc	3	pT2c	3 + 3	ND
29092	71	Adc	4	pT3b	4 + 4	210
29110	69	Adc	4	pT3c	4 + 5	130
29663	50	mAdc	4	pT3b	4 + 5	250
29834	44	Adc	3	pT2c	3 + 4	160
29990	63	Adc	4	pT3a	4 + 3	200
33020	45	Adc	3	pT2c	3 + 4	165
33106	64	mAdc	5	pT3b	5 + 4	180
33072	48	Adc	4	pT3a	4 + 3	200
33120	47	Adc	3	pT2c	3 + 4	200

Table 1. The table shows number of each case, age, prostate cancer type (adc, adenocarcinoma, mAdc, met noma), histological grade, pathological staging based on the pTNM classification, where pT2c indicates bilateral p d total Gleason scores. BMI-1 expression is assessed as the extent of nuclear immunoreactivity by IHC and indicated a H score is obtained using the following formula: H-Score = (% at 0) * 0 + (% at 1+) * 1 + (% at 2+) * 2 + (% at 3- BMI-1 H-score = (3 X percentage of BMI-1 strongly staining nuclei + 2 X percentage of BMI-1 moderately staining nu of BMI-1 weakly staining nuclei), giving a range of 0 to 300. Weak cytoplasmic and/or stromal staining was seen in d was not considered in the score. ND, not determined due to insufficient tissue material.

Task #2. Completed by Bertino Lab.

Task #3. Completed by Sabaawy Lab.

Task #4. Completed by both Sabaawy and Bertino Labs.

Task #5. Completed by both Sabaawy and Bertino Labs.

In **SUMMARY**, our recently published manuscript demonstrated that we have established a platform to utilize 1^{ry} prostate cancer cells from the protectomy tissues that I surgically remove during laparoscopic prostatectomy. We have examined a number of prostate cancer patients with adenocarcinomas and showed that BMI-1/CD44 correlate in high-grade histological and clinical prostate cancer. The partnering PIs have confirmed the activity of C-209 in zebrafish and mouse xenografts. We will continue to collect more primary PCa tissues to study oncogenic addiction of BMI-1 in regulating TICs in primary PCa[2], fish and mouse xenografts, and determine the mechanism of BMI-1 regulation and develop a defined rational for combination therapies during the extension year.

D. KEY RESEARCH ACCOMPLISHMENTS

- We recruited an additional 24 patients with prostate adenocarcinoma, and found increased BMI-1 and CD44 expression in cancer tissues compared to the adjacent normal tissues. These studies will continue with additional patients' tissues in the next year.

- Utilizing primary TICs that we isolated, the partnering PIs identified the first known translational inhibitors of BMI-1 that target prostate TICs.

- These data support a paradigm of therapeutically targeting TICs in prostate cancer with C-209.

- The next stage will be the use of C-209 in combination therapy in xenografts to develop a clinical strategy for the use of BMI-1 inhibitors in prostate cancer therapy.

E. REPORTABLE OUTCOMES

A second manuscript from this award:

Bansal N, Bartucci M, Yussuf S, Davis S, Flaherty K, Huselid E, Patrizii M, Jones D, Cao L, Sydorenko N, Moon Y Zhong H, Medina DJ, Kerrigan J, Stein MN, Kim IY, Davis T, DiPaola RS, Bertino JR, Sabaawy HE. **Selective BMI-1 targeting interferes with patient derived tumor-initiating cell survival and tumor growth in prostate cancer**. *Cell Res.* (submitted). (Manuscript, supplemental material and Editorial and peer review comments are attached in the appendix).

F. CONCLUSION

Prostate tumor-initiating cells (TICs) have intrinsic resistance to current therapies. BMI-1 (B-cell-specific MMLV insertion site-1) regulates stem cell self-renewal, and is over-expressed in TICs. We reported a combined immunophenotypic and time-of-adherence assay to identify human prostate TICs with increased BMI-1 expression. Tumor initiation and dissemination were consistently observed in zebrafish and mouse xenografts in the partnering PIs laboratories. This work also resulted in a publication demonstrating our ability to isolate and propagate primary prostate cancer TICs. My laboratory continued this year to isolate the self-renewing prostate TICs from primary prostate adenocarcinomas. Utilizing the zebrafish and mouse xenografts, the collaborating laboratories on this synergistic award identified the first known translational inhibitors of BMI-1 that target prostate TICs. C-209 reduced the metastatic potential of zebrafish TIC-derived xenografts, and inhibited tumor growth in mouse xenografts, respectively. Therefore, we have accomplished our goal to demonstrate the beneficial effects of targeting prostate TICs with BMI-1 inhibitors. The next phase of studies will further examine the mechanism of BMI-1 targeted therapy in prostate cancer from additional primary tissues, and specifically examine the value of combining TICs-targeted therapy using BMI-1 inhibitors with common therapies targeting the bulk of prostate cancer such as Taxotere and other recently approved therapies in order to develop a therapeutic strategy for prostate cancer treatment by the completion of the project.

G. REFERENCES

1.   Luo J, Zha S, Gage WR, Dunn TA, Hicks JL, Bennett CJ, Ewing CM, Platz EA, Ferdinandusse S, Wanders RJ, Trent JM, Isaacs WB, De Marzo AM. Alpha-methylacyl-CoA racemase: a new molecular marker for prostate cancer. Cancer Res 62:2220-6, (2002). PMC: 11956072.

2.   Bansal N, Davis S, Tereshchenko I, Budak-Alpdogan T, Zhong H, Stein MN, Kim IY, DiPaola RS, Bertino JR, Sabaawy HE. Enrichment of human prostate cancer cells with tumor initiating properties in mouse and zebrafish xenografts by differential adhesion. Prostate, (in press.). PMC:

3.   Jin JK, Dayyani F, Gallick GE. Steps in prostate cancer progression that lead to bone metastasis. Int J Cancer 128:2545-61, (2011). PMC: 21365645.

4.   Dayyani F, Gallick GE, Logothetis CJ, Corn PG. Novel therapies for metastatic castrate-resistant prostate cancer. J Natl Cancer Inst 103:1665-75, (2011). PMC: 21917607.

5.   MacVicar GR, Hussain MH. Emerging therapies in metastatic castration-sensitive and castration-resistant prostate cancer. Curr Opin Oncol 25:252-60, (2013). PMC: 23511665.

6.   Collins AT, Berry PA, Hyde C, Stower MJ, Maitland NJ. Prospective identification of tumorigenic prostate cancer stem cells. Cancer Res 65:10946-51, (2005). PMC: 16322242.

7.   Guo C, Zhang B, Garraway IP. Isolation and characterization of human prostate stem/progenitor cells. Methods Mol Biol 879:315-26, (2012). PMC: 22610567.

8.   Ramaswamy S, Ross KN, Lander ES, Golub TR. A molecular signature of metastasis in primary solid tumors. Nat Genet 33:49-54, (2003). PMC: 12469122.

9.   Danila DC, Heller G, Gignac GA, Gonzalez-Espinoza R, Anand A, Tanaka E, Lilja H, Schwartz L, Larson S, Fleisher M, Scher HI. Circulating tumor cell number and prognosis in progressive castration-resistant prostate cancer. Clin Cancer Res 13:7053-8, (2007). PMC: 18056182.

10.   Fan C, He L, Kapoor A, Gillis A, Rybak AP, Cutz JC, Tang D. Bmi1 promotes prostate tumorigenesis via inhibiting p16(INK4A) and p14(ARF) expression. Biochim Biophys Acta 1782:642-8, (2008). PMC: 18817867.

11.   Fasano CA, Dimos JT, Ivanova NB, Lowry N, Lemischka IR, Temple S. shRNA knockdown of Bmi-1 reveals a critical role for p21-Rb pathway in NSC self-renewal during development. Cell Stem Cell 1:87-99, (2007). PMC: 18371338.

12.   Song LB, Li J, Liao WT, Feng Y, Yu CP, Hu LJ, Kong QL, Xu LH, Zhang X, Liu WL, Li MZ, Zhang L, Kang TB, Fu LW, Huang WL, Xia YF, Tsao SW, Li M, Band V, Band H, Shi QH, Zeng YX, Zeng MS. The polycomb group protein Bmi-1 represses the tumor suppressor PTEN and induces epithelial-mesenchymal transition in human nasopharyngeal epithelial cells. J Clin Invest 119:3626-36, (2009). PMC: 19884659.

13.   Dimri GP, Martinez JL, Jacobs JJ, Keblusek P, Itahana K, Van Lohuizen M, Campisi J, Wazer DE, Band V. The Bmi-1 oncogene induces telomerase activity and immortalizes human mammary epithelial cells. Cancer Res 62:4736-45, (2002). PMC: 12183433.

14.   Liu S, Dontu G, Mantle ID, Patel S, Ahn NS, Jackson KW, Suri P, Wicha MS. Hedgehog signaling and Bmi-1 regulate self-renewal of normal and malignant human mammary stem cells. Cancer Res 66:6063-71, (2006). PMC: 16778178.

15.   Jacobs JJ, Kieboom K, Marino S, DePinho RA, van Lohuizen M. The oncogene and Polycomb-group gene bmi-1 regulates cell proliferation and senescence through the ink4a locus. Nature 397:164-8, (1999). PMC: 9923679.

16.   Cao Q, Mani RS, Ateeq B, Dhanasekaran SM, Asangani IA, Prensner JR, Kim JH, Brenner JC, Jing X, Cao X, Wang R, Li Y, Dahiya A, Wang L, Pandhi M, Lonigro RJ, Wu YM, Tomlins SA, Palanisamy N, Qin Z, Yu J, Maher CA, Varambally S, Chinnaiyan AM. Coordinated regulation of polycomb group complexes through microRNAs in cancer. Cancer Cell 20:187-99, (2011). PMC: 21840484.

17.   Yang MH, Hsu DS, Wang HW, Wang HJ, Lan HY, Yang WH, Huang CH, Kao SY, Tzeng CH, Tai SK, Chang SY, Lee OK, Wu KJ. Bmi1 is essential in Twist1-induced epithelial-mesenchymal transition. Nat Cell Biol 12:982-92, (2010). PMC: 20818389.

18.   Glinsky GV. Death-from-cancer signatures and stem cell contribution to metastatic cancer. Cell Cycle 4:1171-5, (2005). PMC: 16082216.

19.   Berezovska OP, Glinskii AB, Yang Z, Li XM, Hoffman RM, Glinsky GV. Essential role for activation of the Polycomb group (PcG) protein chromatin silencing pathway in metastatic prostate cancer. Cell Cycle 5:1886-901, (2006). PMC: 16963837.

20.   van Leenders GJ, Dukers D, Hessels D, van den Kieboom SW, Hulsbergen CA, Witjes JA, Otte AP, Meijer CJ, Raaphorst FM. Polycomb-group oncogenes EZH2, BMI1, and RING1 are overexpressed in prostate cancer with adverse pathologic and clinical features. Eur Urol 52:455-63, (2007). PMC: 17134822.

21.   Cooper CS, Campbell C, Jhavar S. Mechanisms of Disease: biomarkers and molecular targets from microarray gene expression studies in prostate cancer. Nat Clin Pract Urol 4:677-87, (2007). PMC: 18059348.

22.   Silva J, Garcia V, Garcia JM, Pena C, Dominguez G, Diaz R, Lorenzo Y, Hurtado A, Sanchez A, Bonilla F. Circulating Bmi-1 mRNA as a possible prognostic factor for advanced breast cancer patients. Breast Cancer Res 9:R55, (2007). PMC: 17711569.

23.   Xu W, Zhou H, Qian H, Bu X, Chen D, Gu H, Zhu W, Yan Y, Mao F. Combination of circulating CXCR4 and Bmi-1 mRNA in plasma: A potential novel tumor marker for gastric cancer. Mol Med Rep 2:765-71, (2009). PMC: 21475899.

24.   Zhang X, Wang C, Wang L, Du L, Wang S, Zheng G, Li W, Zhuang X, Dong Z. Detection of circulating Bmi-1 mRNA in plasma and its potential diagnostic and prognostic value for uterine cervical cancer. Int J Cancer 131:165-72, (2011). PMC: 21858805.

25.   Tong YQ, Liu B, Zheng HY, He YJ, Gu J, Li F, Li Y. BMI-1 autoantibody as a new potential biomarker for cervical carcinoma. PLoS One 6:e27804, (2011). PMC: 22132147.

26.   Siddique HR, Parray A, Zhong W, Karnes RJ, Bergstralh EJ, Koochekpour S, Rhim JS, Konety BR, Saleem M. BMI1, stem cell factor acting as novel serum-biomarker for Caucasian and African-American prostate cancer. PLoS One 8:e52993, (2013). PMC: 23308129.

27.   Campbell PJ, Yachida S, Mudie LJ, Stephens PJ, Pleasance ED, Stebbings LA, Morsberger LA, Latimer C, McLaren S, Lin ML, McBride DJ, Varela I, Nik-Zainal SA, Leroy C, Jia M, Menzies A, Butler AP, Teague JW, Griffin CA, Burton J, Swerdlow H, Quail MA, Stratton MR, Iacobuzio-Donahue C, Futreal PA. The patterns and dynamics of genomic instability in metastatic pancreatic cancer. Nature 467:1109-13, (2010). PMC: 20981101.

28.   Gerlinger M, Rowan AJ, Horswell S, Larkin J, Endesfelder D, Gronroos E, Martinez P, Matthews N, Stewart A, Tarpey P, Varela I, Phillimore B, Begum S, McDonald NQ, Butler A, Jones D, Raine K, Latimer C, Santos CR, Nohadani M, Eklund AC, Spencer-Dene B, Clark G, Pickering L, Stamp G, Gore M, Szallasi Z, Downward J, Futreal PA, Swanton C. Intratumor heterogeneity and branched evolution revealed by multiregion sequencing. N Engl J Med 366:883-92, (2012). PMC: 22397650.

29.   Barbieri CE, Bangma CH, Bjartell A, Catto JW, Culig Z, Gronberg H, Luo J, Visakorpi T, Rubin MA. The mutational landscape of prostate cancer. Eur Urol 64:567-76, (2013). PMC: 23759327.

30.   Magee JA, Piskounova E, Morrison SJ. Cancer stem cells: impact, heterogeneity, and uncertainty. Cancer Cell 21:283-96, (2012). PMC: 22439924.

31.   Patrawala L, Calhoun T, Schneider-Broussard R, Li H, Bhatia B, Tang S, Reilly JG, Chandra D, Zhou J, Claypool K, Coghlan L, Tang DG. Highly purified CD44+ prostate cancer cells from xenograft human tumors are enriched in tumorigenic and metastatic progenitor cells. Oncogene 25:1696-708, (2006). PMC: 16449977.

H. APPENDIX

A second manuscript from this award:

Bansal N, Bartucci M, Yussuf S, Davis S, Flaherty K, Huselid E, Patrizii M, Jones D, Cao L, Sydorenko N, Moon Y Zhong H, Medina DJ, Kerrigan J, Stein MN, Kim IY, Davis T, DiPaola RS, Bertino JR, Sabaawy HE. **Selective BMI-1 targeting interferes with patient derived tumor-initiating cell survival and tumor growth in prostate cancer**. Nature Comm. (Under revision). (Manuscript, supplemental material and Editorial and peer review comments are attached in the appendix).

npg manuscripttrackingsystem

Cell Research

| tracking system home | author instructions | reviewer instructions | ⑦ help | tips | ⊠ logout | journal home |

Detailed Status Information

Manuscript #	CR-2015-1231
Current Revision #	0
Submission Date	20th Oct 15
Current Stage	Manuscript Under Consideration
Title	BMI-1 targeting interferes with patient-derived tumor-initiating cell survival and tumor growth in prostate cancer
Running Title	BMI-1 targeting in tumor-initiating cells
Manuscript Type	Original Article
Category	cancer biology, cell cycle, stem cell biology, development, chromatin, epigenetics, transcription
Manuscript Comment	Suggested Reviewers: - Harikrishna Nakshatri, BVSc, DVM, PhD Associate Director, Indiana University Melvin and Bren Simon Cancer Center hnakshat@iupui.edu Expert in cancer stem cells and stem cell biology. - Bruce Boman, MD, PhD, MSPH, FACP Director, Cancer Genetics and Stem Cell Biology Helen F. Graham Cancer Center, Christiana Care brboman@christianacare.org Expert in cancer stem cells and stem cell biology. - Paul P. Liu, MD, PhD Senior Investigator, Genetics and Molecular Biology Branch Head, Oncogenesis and Development Section E-mail: pliu@nhgri.nih.gov Expert in zebrafish and mouse cancer models and drug discovery. - Wafik El-Diery, MD, PhD, FACP Deputy Director, Fox Chase Cancer Center Co-Program Leader, Molecular Therapeutics wafik.eldeiry@gmail.com Expert in cell cycle regulation and stem cell biology. Opposed Reviewers: - Richard White, MD, PhD Memorial Sloan Kettering Cancer Center whiter@mskcc.org Direct competition in zebrafish drug screening studies. - Howard Scher, MD Memorial Sloan Kettering Cancer Center scherh@mskcc.org Direct competition in prostate cancer stem cell studies. - John E Dick, PhD Ontario Cancer Institute

	jdick@uhnres.utoronto.ca Direct competition in BMI-1 targeting studies. - Maarten van Lohuizen, PhD Netherlands Cancer Institute m.v.lohuizen@nki.nl Direct competition in BMI-1 targeting studies.
Corresponding Author	Prof. Hatem Sabaawy (UMDNJ/Robert Wood Johnson Medical School)
Contributing Authors	Dr. Nitu Bansal , Dr. Monica Bartucci , Dr. Shamila Yusuff , Dr. Stephani Davis , Mrs. Kathleen Flaherty , Mr. Eric Huselid , Mr. Michele Patrizii , Mr. Daniel Jones , Dr. Liangxian Cao , Dr. Nadiya Sydorenko , Dr. Young-Choon Moon , Dr. Hua Zhong , Prof. Daniel Medina , Dr. John Kerrigan , Dr. Mark Stein , Prof. Isaac Kim , Dr. Thomas Davis , Prof. Robert DiPaola , Prof. Joseph Bertino
Abstract	Current prostate cancer (PCa) management calls for identifying novel and more effective therapeutic approaches. Self-renewing tumor-initiating cells (TICs) hold intrinsic therapy-resistance and account for tumor relapse and progression. BMI-1 regulates stem cell self-renewal, thus impairing BMI-1 function for TICs-tailored therapies appears to be a promising approach. We have previously developed a combined immunophenotypic and time-of-adherence assay to identify CD49bhiCD29hiCD44hi cells as human prostate TICs. Here we show that in TICs, BMI-1 expression is upregulated and associated with stem cell-like traits. Pharmacological inhibition of BMI-1 in patient-derived cells significantly decreased colony formation in vitro and attenuated tumor initiation in vivo, thereby functionally diminishing the frequency of TICs. Furthermore, BMI-1 inhibition, while displaying antitumor activity in both zebrafish and mouse xenografts, did not exert toxic effects on normal tissues. These data offer a paradigm for targeting TICs and support the development of BMI-1-related therapy for more effective PCa treatment.
Editor	Jingjing Zheng
Keywords	BMI-1, Tumor initiating cells
Techniques	Life sciences techniques, High throughput screening [Small molecule library]; Life sciences techniques, Cell/tissue technologies [Stem cells]; Life sciences techniques, Experimental organisms [Zebrafish]; Life sciences techniques, Protein techniques [Protein expression]; Life sciences techniques, Signal transduction techniques [Flow cytometry]; Life sciences techniques, Signal transduction techniques [Tissue culture];
Subject Terms	Biological sciences/Cancer/Cancer therapy/Targeted therapies Biological sciences/Cancer/Urological cancer/Prostate cancer Biological sciences/Developmental biology/Self-renewal
Duality of Interest	There is no duality of interest
Funding Body Archiving Mandates	Funding Summary
Applicable Funding Source	U.S. Department of Defense (DOD) - W81XWH-12-1-0249 [Sabaawy] HHS	NIH	National Cancer Institute (NCI) - P30 CA072720 [Sabaawy] Wellcome Trust - 092687 [Sabaawy]

Stage	Start Date
Manuscript Under Consideration	21st Oct 15
Editor Assigned	21st Oct 15
Manuscript Received	20th Oct 15

eJournalPress

BMI-1 targeting interferes with patient-derived tumor-initiating cell survival and tumor growth in prostate cancer

Nitu Bansal[1,§], Monica Bartucci[1,§], Shamila Yusuff[1], Stephani Davis[2], Kathleen Flaherty[1], Eric Huselid[2], Michele Patrizii[2], Daniel Jones[3], Liangxian Cao[4], Nadiya Sydorenko[4], Young-Choon Moon[4], Hua Zhong[5], Daniel J. Medina[1,6], John Kerrigan[1], Mark N. Stein[1,6], Isaac Y. Kim[1,7], Thomas W. Davis[4], Robert S. DiPaola[1,6], Joseph R. Bertino[1,2,6*], Hatem E. Sabaawy[1,2,3,6*]

[1]Rutgers Cancer Institute of New Jersey, Rutgers University, New Brunswick, NJ 08901.

Graduate Program in [2]Cellular and Molecular Pharmacology and [3]Cell and Developmental Biology, RBHS-Robert Wood Johnson Medical School, Graduate School of Biomedical Sciences, Rutgers University, New Brunswick, NJ 08901.

[4]PTC Therapeutics, Inc., 100 Corporate CT, South Plainfield, NJ 07080.

Departments of [5]Pathology and Laboratory Medicine, [6]Medicine and [7]Surgery, RBHS-Robert Wood Johnson Medical School, Rutgers University, New Brunswick, NJ 08901.

[§] These authors contributed equally.

*Corresponding authors:

J R Bertino, M.D.

Cancer Institute of New Jersey, 195 Little Albany Street, Room 3033, New Brunswick, NJ 08901, USA. Telephone: 732-235-8510

Email address: bertinoj@cinj.rutgers.edu

H E Sabaawy, M.D., Ph.D.

Cancer Institute of New Jersey, 195 Little Albany Street, Room 4557, New Brunswick, NJ 08901, USA. Telephone: 732-235-8081

Email address: sabaawhe@cinj.rutgers.edu

Running Title: BMI-1 targeting in tumor-initiating cells

Key words: Prostate cancer stem cells, tumor-initiating cells, BMI-1, zebrafish

Text word count: 4,864

Abstract word count: 150

Abstract

Current prostate cancer (PCa) management calls for identifying novel and more effective therapeutic approaches. Self-renewing tumor-initiating cells (TICs) hold intrinsic therapy-resistance and account for tumor relapse and progression. BMI-1 regulates stem cell self-renewal, thus impairing BMI-1 function for TICs-tailored therapies appears to be a promising approach. We have previously developed a combined immunophenotypic and time-of-adherence assay to identify CD49b^{hi}CD29^{hi}CD44^{hi} cells as human prostate TICs. Here we show that in TICs, BMI-1 expression is upregulated and associated with stem cell-like traits. Pharmacological inhibition of BMI-1 in patient-derived cells significantly decreased colony formation *in vitro* and attenuated tumor initiation *in vivo*, thereby functionally diminishing the frequency of TICs. Furthermore, BMI-1 inhibition, while displaying antitumor activity in both zebrafish and mouse xenografts, did not exert toxic effects on normal tissues. These data offer a paradigm for targeting TICs and support the development of BMI-1-related therapy for more effective PCa treatment.

Introduction

Prostate cancer (PCa) is the most common cancer affecting men in the developed world [1]. Current treatments are only temporarily effective, and therapy resistance and relapse are commonly inevitable [2]. We and others have shown that primary PCa contain cells endowed with self-renewal and tumorigenic potential [3-8], known as tumor-initiating cells (TICs) [9]. By virtue of their resistance to therapy, TICs could be the prime cause of tumor relapse. Thus, in order to accomplish tumor eradication, efforts are made to design TIC-tailored therapy that would selectively target these highly aggressive tumorigenic cells.

An attractive treatment strategy is to use agents capable of impeding the self-renewal abilities of TICs, therefore targeting heterogeneous cells in all tumor clone(s) within a given patient. BMI-1 (B-cell specific MMLV insertion site-1), a member of the polycomb family of the chromatin remodeling complex, was shown to regulate stem cell self-renewal [10] and play a key role in PCa initiation and progression [11]. In clinical specimens, BMI-1 expression correlates with high rates of PCa recurrence [12], and downstream targets of the BMI-1 are associated with therapy-resistant PCa [13]. These data closely associate BMI-1 with the presence of tumor-initiating stem-like cells in clinical PCa samples, making it reasonable to assume that small-molecule inhibitors targeting BMI-1 could be the first in a new class of antitumor therapy directed against self-renewing and chemo-resistant TICs.

Previously, we developed a surrogate self-renewal assay that allowed us to isolate TICs from PCa tissue based on $\alpha2\beta1$-integrin (also called CD49b/CD29) and CD44 protein expression [6]. Herein, we investigated the role of BMI-1 in human prostate TICs. We demonstrate that in prostate TICs, BMI-1 is overexpressed and functionally regulates their survival and maintenance. Targeting of BMI-1 with a novel inhibitor impaired self-renewal and migratory

potential *in vitro.* Consistently, BMI-1 inhibition *in vivo* decreased tumor growth and significantly reduced TICs in patient-derived samples and tumor xenografts, as evaluated by CD49b/CD29/CD44 staining, serial transplantation *in vivo* and clonogenic prostasphere assays *ex-vivo.* Remarkably, these outcomes were not observed following conventional chemotherapy treatments. Given the role of TICs in resistance to current therapies, these observations support the evaluation of BMI-1 inhibitors for more effective PCa management.

Results

BMI-1 is a potential target for human prostate TICs

BMI-1 is a key player in PCa initiation, recurrence and progression [11, 12]. Accordingly, we found that BMI-1 is differentially expressed in PCa cell lines, but low in normal prostate epithelial cells (Supplementary information, Figure S1A). To assess the functional role(s) of BMI-1 in PCa, we performed BMI-1 loss-of-function analyses in DU145 PCa cells (Supplementary information, Figure S1B). Downregulation of BMI-1 was associated with decreased cell motility and clonogenic capability, as well as potentiated chemosensitivity (Supplementary information, Figure S1C, S1D and S1E). Notably, resistance to drug-induced apoptosis, motility, invasiveness and clonogenicity have been traced to TICs [14].

We recently found that in PCa, clonogenic, migratory and *in vivo* tumorigenic potentials are enriched in the collagen-I rapidly adherent (5min) $CD49b^{hi}CD29^{hi}CD44^{hi}$ cell population [6], identified therefore as TICs. Thus, we utilized this phenotypic and functional adherence assay to analyze BMI-1 expression (Figure 1A). Indeed, the rapidly adherent DU145 cells were enriched in the $CD49b^{hi}CD29^{hi}CD44^{hi}$ phenotype (Figure 1B and 1C), and significantly overexpressed BMI-1, both at the RNA (Figure 1D) and protein levels (Figure 1E and 1F, and Supplementary information, Figure S2A). Furthermore, as expected, the rapidly adherent $CD49b^{hi}CD29^{hi}CD44^{hi}$ TICs were enriched for the other prostate TIC markers integrin-α6 (CD49f) and TROP; [4, 8] (Supplementary information, Figure S2B), suggesting that BMI-1 is enhanced in the more tumorigenic cell compartment [6] of PCa. To further confirm our results and model, we also assessed BMI1 expression upon sorting of the high and low CD49CD29CD44 cells and found the same outcomes (Supplementary information, Figure S2C).

To study whether BMI-1 expression modulates the levels of TICs, we employed the collagen adherence assay after lentiviral-mediated knockdown. Loss of BMI-1 in sh-BMI-1 DU145 cells resulted in a significant (~40%) decrease in the numbers of rapidly adherent CD49b^{hi}CD29^{hi}CD44^{hi} cells (Figure 1G), suggesting an impact of BMI-1 on the TIC population.

Identification of pharmacological BMI-1 inhibitors

We previously demonstrated that BMI-1 expression is tightly controlled by post-transcriptional processes mapping to the 5'- and 3'-untranslated regions (UTRs) [15]. In reporter cells containing the luciferase open reading frame flanked with the human BMI-1 5'- and 3'-UTRs, the BMI1 3´-UTR enhanced BMI-1 expression, while the internal ribosome entry site (IRES)-containing 5'-UTR impaired BMI-1 expression and controlled the effect of the 3'-UTR [15].

These observations allowed the construction of a platform to identify compounds impacting the regulatory mechanisms within the BMI-1 5`UTR and 3`UTR to modulate BMI-1 protein expression [15, 16].

A high-throughput screen against a library of >200,000 small molecules (PTC Therapeutics) identified seven compounds, with the same core structure (Figure 2A), targeting the post-transcriptional control mechanisms described above [15, 16]. To examine their antitumor activity, we determined their IC$_{50}$ concentrations in total DU145 cells (Supplementary information, Figure S3A). Among them, three compounds: C-209, C-210 and C-211

significantly decreased the number of rapidly adherent CD49b^{hi}CD29^{hi}CD44^{hi} cells by an average of 30-50% (Figure 2B).

BMI-1 enables transcriptional repression of >1,600 target genes through the PRC1 complex [17], therefore, targeting BMI-1 would evoke complex cellular responses depending on the cell type and/or activated pathways. We evaluated BMI-1 protein inhibition by ELISA and Western blotting in comparison to EZH2; a closely related PRC2 protein with a similarly short half-life [18]. Indeed, all three compounds reduced BMI-1 expression in a dose-dependent manner (Figure 2D), but had no effects on EZH2 (Figure 2D).

Furthermore, BMI-1 knockdown induces senescence [10]. Treatment of mouse embryonic fibroblasts (MEFs), that are either Bmi-1$^{+/+}$ or Bmi-1$^{-/-}$, with C-209, C-210 and C-211 respectively, elicited a significant dose-dependent increase in senescence in Bmi-1$^{+/+}$ MEFs, and sh-BMI-1 DU145 cells, but not in the highly senescent Bmi-1$^{-/-}$ MEFs (Supplementary information, Figure S3B and S3C), suggesting a potential functional specificity of the selected inhibitors in targeting BMI-1's effects on cellular senescence.

Pharmacological targeting of BMI-1 in human prostate TICs

To establish that BMI-1 inhibition has activity against the putative TICs in PCa, we treated different PCa cells with C-209. This treatment significantly impaired the percentage of rapidly adherent CD49b^{hi}CD29^{hi}CD44^{hi} (TICs) (Figure 2E and 2F), induced a G1 cell cycle accumulation (Supplementary information, Figure S3D), which was anticipated from loss of BMI-1's cell cycle regulatory function(s) [19], reduced number of cells in S phase (Supplementary information, Figure S3D) and critically, evoked a dose-dependent reduction in both BMI-1 and C-terminal lysine-119 mono-ubiquitinated form of γ-H2A, a specific

product of the BMI-1 PRC1 complex activity [19] (Supplementary information, Figure S3E and S3F).

Self-renewal capacity is a distinguishing property of stem cells. Serial clonogenic spheroid assays could estimate the frequency of TICs, especially after treatments [20]. To evaluate the ability of these compounds to target serial clonogenic capacity, single cells collected from primary spheroids were plated in the presence of C-209, C-211 and two commonly used chemotherapies, methotrexate and doxorubicin. Unlike the initial slight inhibitory effects of methotrexate and doxorubicin, treatment with C-209 and C-211 considerably diminished the number of single cell-derived secondary spheroids, and more importantly tertiary spheroids (Figure 2G). While methotrexate had no effect, the outcomes of C-209 and C-211 treatment were remarkable, as nearly a 10-fold reduction was observed (Figure 2G). We therefore hypothesized that inhibiting BMI-1 might eliminate self-renewing, hence more tumorigenic cells, chemotherapies only affect the proliferating transit-amplifying cells sparing the ones endowed with clonogenic capacities, and characterized by a lower proliferative kinetic. In line with this notion, serial spheroid formation in presence of the general protein biosynthesis inhibitor cycloheximide (CHX) [21], similar to chemotherapies, did not impact cells capable of self-renewal (Figure 2G), thus corroborating our hypothesis.

Effects of BMI-1 inhibition on normal cells

When targeting TICs, an important concern is the effect on "normal" cell compartments. Zebrafish embryos, are valuable models for *in vivo* drug toxicity studies [22].

In toxicological assays, C-209, C210, and C-211 had no notable effects on zebrafish development at their respective IC_{50s} (Supplementary information, Figure S4A). However, at higher doses, C-210 and C-211 impeded embryo hatching and caused embryo curling, thus suggesting narrow safety margins (Supplementary information, Figure S4A and S4B). In contrast, zebrafish embryonic development and survival were not impacted by C-209 treatment at the IC_{50} conc. (Supplementary information, Figure S4B). These data prompted us to dismiss C-210 and 211 inhibitors and focus on establishing the safety profile of C-209. To provide evidence that the effects of C-209 were not related to a general disruption of mRNA translation, zebrafish embryos were exposed in parallel to the universal translational inhibitor CHX (Supplementary information, Figure S5A). CHX treatment resulted in developmental arrest and profound embryonic toxicity at low concentrations, while embryos treated with C-209 at 3µM survived and progressed normally throughout development (Supplementary information, Figure S5A). Likewise, treatment of adult zebrafish with C-209, but not CHX, yielded no apparent impact on survival (Supplementary information, Figure S5B).

To further assess C-209 adverse effects on normal mammalian tissues, BMI-1 inhibition was also tested on normal prostate epithelial RWPE1 cells by examining clonogenic potential pre- and post-C-209 treatment. While C-209 drastically reduced DU145 PCa colony formation, RWPE1 cells, while showing an expected much lower clonogenic proclivity than DU145 cancer cells, BMI-1 inhibition was mostly ineffective (Supplementary information, Figure S6A).

Furthermore, because self-renewal of hematopoietic stem and progenitor cells (HSPCs) is vital for the sustained production of blood cells [10], we evaluated the clonogenic capacity of primary

human CD34^{+} HSPCs upon treatment with C-209 and observed no significant effect (Supplementary information, Figure S6B). Additionally, treatment of mice with C-209 did not induce any anemia and/or thrombocytopenia, nor histological changes were observed in the bone marrow of treated *vs.* untreated mice (Supplementary information, Figure S6C), suggesting that dosage limited targeting of BMI-1 might have more effective role(s) in inhibiting the clonogenic potential of tumor versus normal stem cells.

C-209 could target post-transcriptional regulation of BMI-1

To gain insight into the mechanism of action of C-209 (Figure 3A) against PCa, We assessed the electrostatic potential of C-209 (Figure 3B), and then used the UCSF DOCK program to model the docking of C-209 to the human BMI 5´UTR RNA. The docking model suggests that C-209 could bind to pockets formed in the BMI-1 RNA fold structures (Figure 3C). We next utilized the BMI-1 UTR luciferase reporter constructs (Figure 3D), previously used to demonstrate the regulatory roles of BMI-1 UTRs [15], to examine the effects of C-209 on cells harboring these BMI-1 UTR regulatory reporters. Indeed, C-209 treatment significantly reduced normalized luciferase expression in DU145 cells harboring the BMI-1 3`UTR and reversed the BMI-1 expression repressing effects [15] of the IRES-containing BMI-1 5`UTR (Figure 3E). Thus, in PCa cells, C-209 engages the BMI-1 regulatory mechanisms embedded within the UTRs.

We next performed time course experiments in DU145 and PC3 PCa cells (Figure 3F), and observed that C-209-mediated downregulation of BMI-1 occurs between 48-72hrs, depending on the cell type (Figure 3F). To examine if C-209 is selective for BMI-1 post-transcriptional inhibition, we utilized control and BMI-1 UTRs reporter cells and found that C-209

preferentially inhibit expression of a reporter, the translation of which is under the BMI-1 5`-

and 3`UTR control, rather than alternate control UTRs (Figure 3G). We also treated DU145

cells concomitantly with C-209 2μM and CHX, a general translational inhibitor, and analyzed

mRNA expression of BMI-1 and the CHX target epithelial sodium channel (αENaC) [23].

While treatment with CHX mutually lowered mRNA levels of both BMI-1 and αENaC, C-209

exposure did not exert a lowering effect on the levels of transcribed BMI-1 mRNA (Figure

3H). In contrast, C-209 caused a slight increase in the BMI-1 message, explained by a

reported cellular addiction to BMI-1 [11, 12, 24], followed by decreased BMI-1 protein level

when compared to untreated or CHX treated DU145 cells (Figure 3H and 3I). Thus, C-209

reduces the production of BMI-1 protein likely by modulating its post-transcriptional

regulation.

Nonetheless, to specifically link C-209 effects to targeting post-transcriptional regulation of

BMI-1 transcripts, we analyzed BMI-1 translation directed by full-length (UTR-containing)

human BMI-1 cDNA [25] in eukaryotic cell-free expression system. Incubation of the BMI-1

cDNA with C-209 for just one hour before translation decreased BMI-1 protein synthesis by

27% (Figure 3J).

Moreover, we performed a dose-response cell viability assay in BMI-1-deficient (sh-BMI-1) and

BMI-1-overexpressing (EGFP BMI-1) DU145 cells, and compared the results to control

transduced DU145 Sh-Scr cells expressing endogenous level of the protein (Figure 3K). Unlike

DU145 Sh-Scr cells, whose survival was impaired even at low C-209 doses (IC$_{50}$ 1.25-

2.5 μM), both DU145 BMI-1-deficient (lacking the target) and -overexpressing (with excess

target) cells showed a lower sensitivity, being affected only at very high concentrations of C-

209 (DU145 EGFP-BMI-1 IC_{50} ~10μM and DU145 sh-BMI-1 IC_{50} ~15μM). Survival analyses

comparison between DU145 Sh-Scr and DU145 sh-BMI-1 cells revealed a highly significant

response of DU145 Sh-Scr cells to C-209 even starting at 0.3125 μM (Figure 3L). Accordingly,

in order to experience the growth-inhibitory effect of C-209, BMI-1-overexpressing cells

required a higher dose than DU145 Sh-Scr (Figure 3L), therefore providing another evidence

that C-209 effects could be selective towards BMI-1 targeting.

Also, to examine other potential mechanisms of action, C-209 activity was examined against a

panel of 245 kinases and 21 phosphatases. These assays elucidated a lack of significant

inhibition (data not shown).

BMI-1 inhibition in patient-derived TICs

To assess the value of a new treatment, primary patient-derived cells represent a much more

relevant model compared to cell lines. Despite the known difficulties in culturing primary PCa

cells *in vitro*, even if for brief periods, we have recently successfully maintained primary PCa

cells endowed with self-renewal and *in vivo* tumorigenic potential in culture [6]. Therefore, we

examined C-209 treatment in a panel of short-term cultures from primary PCa cells

differentially expressing BMI-1 (Table S1 and Supplementary information, Figure S7).

Exposure of patient-derived PCa cells to C-209 resulted in significant BMI-1 downregulation

(Figure 4A) followed by antitumor activity at an IC_{50} lower but not significantly different

from that found in DU145 cells (Figure 4B). Notably, a significant downregulation of BMI-1

was not observed in patient-derived normal counterparts treated with C-209 (Figure 4A).

Remarkably, as observed with tumor cell lines, treatment with C-209 caused a critical

reduction in the rapidly adherent $CD49b^{hi}CD29^{hi}CD44^{hi}$ (TIC) population in primary PCa

cultures (Figure 4C, left and right panels). In contrast, treatment with docetaxel, a first line treatment for advanced PCa [2], resulted in enrichment of the highly aggressive CD49b^{hi}CD29^{hi}CD44^{hi} TICs.

The effectiveness of any targeted therapy is based on the absence of relapse and/or secondary clonal lesions [26]. Since TICs account for tumor progression by the virtue of their treatment-resistance, self-renewal and tumor-seeding capacity [14], it is reasonable to deduce that the efficacy of a TIC-tailored strategy relies on a diminished clonogenic and tumorigenic capacity.

In order to evaluate C-209 efficiency in targeting patient-derived TICs, we pre-treated distinct primary PCa cells for several days with either C-209 or docetaxel. Subsequently, to investigate the long-term impact of treatments, particularly in a post therapy discontinuation setting, cells were washed and replated. Cell rescue and soft agar assays were assessed to evaluate differences in cell survival and colony-forming repopulation abilities. Interestingly, both docetaxel and C-209 treatments impaired short-term survival of primary PCa, although C-209 to a more significant extent (Figure 4D). Critically, patient-derived PCa cells maintained the ability to form colonies after single treatments with docetaxel but significantly less with C-209 (Figure 4E), indicating that BMI-1 inhibition impairs survival and clonogenic activity of primary PCa TICs.

BMI-1 has been implicated in PCa metastasis [27]. Since loss of function of BMI-1 impaired PCa cell migration (Supplementary information, Figure S1C), we assessed the post-treatment propensity of patient-derived PCa cells to migrate in modified Boyden chambers. We found that, while docetaxel–treated cell migratory potential was almost unchanged, C-209-exposure

significantly diminished their motility (Figure 4G), thus suggesting a notable role for BMI-1 in cancer dissemination.

Evaluation of C-209 in vivo

Successful murine xenografting of primary human PCa, in the absence of inducing murine urogenital mesenchyme [28], has rarely been achieved. We have shown that embryonic and juvenile zebrafish could be successfully used as PCa xenograft models [6]. Here, we utilized these xenografts to identify small molecule inhibitors that functionally target BMI-1 and self-renewal activities (Figure 5A). We isolated PCa cells from twenty-four patients undergoing surgical prostatectomy (Table S1), and examined their tumor initiation potential in zebrafish xenografts. PCas were diagnosed based on histological examination (Figure 5B, 5C, and 5D). The expression of the PCa-specific alpha-methylacyl coenzyme-A racemase (AMACR) when combined with overexpression of Erg [29], provide excellent dual PCa-specific biomarkers [6] (Figure 5E, 5F, and 5G, and Supplementary information, Figure S8A and S8B). We detected Erg overexpression associated with AMACR in the mirror sections of sampled PCa tissue (Figure 5E, 5F, and 5G), and within zebrafish xenografts (Supplementary information, Figure S8C, S8D, and S8E), in cells that expressed the human isoform of CD44 and BMI-1 (Supplementary information, Figure S8F, S8G, and S8H). TICs isolated from primary PCa engrafted robustly in the pre-immune zebrafish embryos (Figure 5H), forming xenografts (Figure 5H, 5I, 5G, and 5K) with cells morphologically similar to the patient's biopsy cells (compare cells in Figure 5D to those in Figure 5K) and positive for Prostatic Specific Antigen (PSA) staining (Figure 5L, 5M, 5N, and 5O).

Again, we employed the zebrafish toxicity assay to demonstrate that the compounds under investigation have no notable toxicities when used at their corresponding IC_{50s} (Supplementary information, Figure S9A and S9B). We next treated zebrafish embryos that were engrafted with quantum dot (QD)-labeled TIC-derived PCa (Figure 6A and Supplementary information, Figure S10A). Treatment of PCa xenografts from multiple patient samples (Figure 6C and 6D) with C-209 at 2μM led to tumor shrinkage (Figure 6B and 6D, and Supplementary information, Figure S10B, left and right panels). Likewise, treatment of juvenile xenograft fish with C-209 led to tumor reduction (Supplementary information, Figure S10C, left and right panels), suggesting that although governing the cell fate of TICs, BMI-1 likely regulates the viability of PCa cells in general.

To determine C-209 efficacy in targeting TICs, hence tumor reinitiation, primary PCa were treated with either docetaxel or C-209 for few days before being washed and injected into zebrafish embryos. After 10 days, C-209-treated cells gave rise to significantly less tumors than control- or docetaxel-treated cells (Figure 6E). Notably, these effects were associated with a significant reduction in Ki67 staining (Figure 6F).

Xenotransplantation, followed by serial repopulation, is considered an essential criterion to assess serial maintenance of stemness in defining TICs. Thus, we sorted labeled pooled tumor cells from primary zebrafish xenografts treated either with DMSO or C-209, and used them for secondary xenografts (Figure 6G). TICs from DMSO-treated embryos were able to initiate secondary grafts in 81.8% of cases (n=54/66 secondary xenograft embryos from three patient samples), while C-209-treated cells had significantly less tumor initiation potential in only 29.3% of cases (n=22/75 from three patient samples) (p<0.001) (Figure 6G), suggesting that C-209 treatment is effectively impairing the frequency of TICs in zebrafish xenografts.

Moreover, because we observed that BMI-1 affected cell motility potential *in vitro*, we performed histological analyses on localized and metastatic sections of zebrafish xenografts. Primary tumors, identified through expression of human CD44 [6], had <50% of BMI-1 expressing cells, in contrast to >90% of BMI-1 positive cells in metastatic colonies (Figure 6H and 6I), suggesting that metastatic tumors might contain a larger fraction of TICs expressing BMI-1 and/or that BMI-1 might play a prominent role in cancer dissemination.

Zebrafish provide a powerful organism to study the cancer self-renewal population [30]. To examine whether C-209 treatment affects tumor response and TIC survival in a murine model, we employed a strategy aimed at unraveling the targeting of self-renewing TICs (Figure 7A). We injected rapidly adherent $CD49b^{hi}CD29^{hi}CD44^{hi}$ DU145 TICs [6], that were previously infected with a lentiviral vector encoding luciferase2/enhanced green fluorescent protein (Luc2/EGFP), into NOD-SCID-IL-2R null (NSG) mice. Tumors, allowed to grow until the size of ~100 mm^3, were treated with C-209 or the chemotherapeutic agent docetaxel for ~2 weeks (Figure 7B). At the end of treatments, while vehicle-treated tumors grew exponentially and docetaxel exerted a minimal effect on xenografts growth, C-209-treated tumors were significantly inhibited (Figure 7B). Additionally, since tumor relapse is frequently observed following treatment discontinuation, tumor volume was monitored with an electronic caliper for additional 15 days. Noticeably, at the end of this period, the results in Figure 7B, while revealing a significant difference in tumor growth between docetaxel-treated and untreated mice, show an even higher disparity in C-209-treated xenografts, thus, corroborating the efficiency of anti-BMI-1-based therapy.

Severe tumor damage indicated by the large necrotic areas was present two weeks after the last

delivery of chemotherapy and C-209 (Figure 7C). In line with this, Ki67+ cells in grafts with reduced nuclear BMI-1 and surface CD44 expression from C-209 treated mice were significantly lower when compared to controls (Figure 7D and 7E).

To investigate whether C-209 treatment was able to target TICs *in vivo,* clonogenic assays *ex vivo* and serial transplantations were assessed from treated and untreated xenografts (Figure 7A). Interestingly, the clonogenic potential of cells dissociated from C-209-treated tumors was significantly reduced (Figure 7F). To determine the frequency of cells having clonogenic, hence tumorigenic function, in the mixed tumor bulk population, we performed *ex vivo* a limiting dilution assay between C-209-treated and untreated xenograft-derived cells. While control-derived cells were highly clonogenic, C-209-treated xenograft-derived cells generated colonies at a lower frequency (Supplementary information, Figure S11). Importantly, while both control- and docetaxel-xenograft derived cells could be serially transplanted in secondary recipients, the graft repopulation of C-209-treated tumors was significantly reduced (Figure 7G), thus demonstrating that BMI-1 targeting is effective against tumor-propagating cells.

Collectively, our data demonstrate that C-209, a novel small molecule that targets post-transcriptional regulation of BMI-1, displays mutually effective anti-TICs and antitumor activities in both zebrafish and mouse PCa xenografts.

Discussion

Mounting evidence support the notion that distinct tumor subpopulations termed cancer stem cells (CSCs) or TICs as responsible for tumor generation and treatment failure [31, 32]. Accordingly, to achieve tumor eradication, we need new approaches capable of targeting the tumorigenic core of cancers. TICs possess indefinite replicative ability due to an inherent or acquired self-renewal capacity. Consequently, targeting self-renewal potential of a given tumor may be the key towards developing more effective treatments.

Multiple molecular pathways regulate the self-renewal potential of stem cells and are therefore potential targets in TICs [33]. Among these, BMI-1, the key component of PRC1 transcriptional repressor complex that plays important roles in cell cycle regulation and cellular senescence, represents a most critical target. BMI-1 is in fact also necessary for Hh- [34], β-catenin- [35], and Akt-mediated self-renewal [24, 36], thus is a key stem cell self-renewal regulator [36]. In PCa, BMI-1 activation occurs in primary tumors [27], transgenic mice [11, 24] and in stem cells from metastatic PCa with poor prognosis [13]. Additionally, the expression of BMI-1 in PCa is highly predictive of PSA recurrence [12]. BMI-1 thus is a critical target regulating the proliferative activities of prostate TICs and PCa overall.

Here, we initially demonstrated that knockdown of BMI1 impairs stem cell-like traits in PCa, likely by reducing TICs frequency. Next, through high-throughput followed by selective approaches, we identified a small molecule that targets BMI-1 post-transcriptional regulation and investigated its ability to interfere with TIC survival and self-renewal capacity.

Human prostate spheroids have increased BMI-1 [37]. Herein we showed that, in the 5min adherent $CD49b^{hi}CD29^{hi}CD44^{hi}$ tumorigenic stem-like cells, BMI-1, Integrin-α6 (CD49f) and TROP2 levels are higher than in the non-tumorigenic counterpart. Moreover, BMI-1 protein is highly

enriched in these 5min adherent CD49b^{hi}CD29^{hi}CD44^{hi} cells. Colony, serial spheroid formation and tumor xenograft studies showed that BMI-1 controls self-renewal, hence tumor-seeding capacity of prostate TICs. Importantly, the same outcomes were not observed with conventional chemotherapies or general translational inhibitor treatments. These data suggest that, unlike chemotherapies, which largely spare and even enrich cells endowed with tumorigenic capacities [31], exposure to C-209 efficiently reduces the survival and clonogenic potential of TICs in PCa. Likewise, C-209 impaired TIC-associated features alongside with survival of PCa cells in zebrafish and mouse PCa xenografts.

A possible drawback for the development of agents targeting stem cell self-renewal may be the potential toxicity deriving from inhibition of normal differentiation, particularly in HSPCs [38]. Importantly, C-209 had less of an effect on CD34$^+$ HSPCs. The *in vivo* administration of C-209 did not alter bone marrow integrity, nor did it induce anemia and/or thrombocytopenia in treated mice. Additionally, no notable toxicity was observed in zebrafish at the IC$_{50}$ employed. These findings suggest that it might be possible to target TICs overexpressing BMI-1 with lower doses of targeted therapy, and without notable toxic effects on normal cells. Indeed, we have recently demonstrated that lower doses of AKT-targeted therapy could target and radiosensitize glioblastoma TICs overexpressing BMI-1 [36].

Tumor regrowth is often observed in cancer patients following chemotherapy withdrawal. We found C-209 treatment interruption did lead to a rapid tumor growth rebound. Thus, targeting BMI-1 by C-209 treatment could be exploited to devise more effective therapeutic approaches for PCa. Importantly, the significant reduction in clonogenic cells in C-209-treated grafts, proved by limiting dilution and clonogenic assays *ex-vivo*, and the reduced serial transplantation

capacity of xenograft-derived cells, suggest that such treatment impairs the survival of TICs, which, in contrast, were largely spared by docetaxel treatment. BMI-1 may also cooperate in regulating epithelial-to-mesenchymal transition (EMT) [39], a state associated with TICs and metastasis. We found BMI-1 to be overexpressed in secondary tumor lesions, also BMI-1 inhibition was accompanied by reduced cell motility in PCa, therefore a link may exist between BMI-1-expressing self-renewing TICs and cancer dissemination in PCa.

ChIP-Seq and global mapping revealed that BMI-1 transcriptionally represses ~1,600 targets through the PRC1 complex, with many targets vastly involved in apoptotic and cell survival pathways [40], therefore driving the proliferation-promoting function of BMI-1 [41].

C-209 was identified in a screen utilizing reporter cells that harbor BMI-1 5`UTR and 3`UTR. Treatments of tumor cells with C-209 reduced BMI-1 protein levels but not EZH2 nor a panel of 245 kinases and 21 phosphatases, increased cellular senescence, reduced the specific BMI-1 product of activity lysine-119 mono-ubiquitinated form of γ-H2A [19], induced a G1 cell cycle accumulation, and impaired TICs by abolishing serial spheroid formation *in vitro* and graft repopulation potential *in vivo,* altogether are functional effects suggesting that C-209 may directly or indirectly targets BMI-1 to evoke a complex cellular response.

Structure activity relationship in UTR reporters and modeling studies suggest that C-209 could be relatively selective towards targeting the BMI-1 transcript, harboring the BMI-1 UTR regulatory elements. Thus, the anti-proliferative effects of C-209 could be due to direct modulation of BMI-1 post-transcriptional control mechanisms regulating BMI-1 translation and embedded within the UTRs, such as control of translation initiation either directly in a cap-independent fashion or

possibly through riboswitches, which also control splicing in the 3`UTR by coupling metabolite

binding to mRNA processing, or indirectly by regulating mRNA stability [42].

Few small molecules are known to elicit their effects by modulating RNA function(s) outside of

the bacterial ribosome. Although the exact site(s) on the BMI-1 5`UTR and/or 3`UTR targeted by

C-209 remains to be determined, and detailed binding studies are necessary to delineate the exact

selectivity of C-209 towards BMI-1, absolute selectivity is not necessarily the best approach when

considering BMI-1 inhibition as a potential treatment for PCa, because high selectivity could lead

rapidly to resistance.

Genetic modulation of BMI-1 in PCa cell lines revealed a linear correlation between protein

expression and the anti-proliferative as well as anti-TIC response to C-209. Instead, tumors from

different patients exhibit variegated responses, due to their extensive heterogeneity [43] that,

unlike immortalized cell lines [44], are derived from distinct genetic alterations and cell

proliferation kinetics.

Mutations, such as those affecting AR signaling and PTEN/PI3K/AKT activation, could render

PCa cells addicted to the activity of BMI-1 signaling, and will therefore delineate responses to

therapy. For instance, ectopic overexpression of Bmi-1 in the mouse prostate gland, together

with ablation of PTEN, results in aggressive PCa, that become dependent on Bmi-1 [24].

Addiction of PCa cells to BMI-1 likely activates cellular signals in tumor cells, which are absent

in normal tissue, to elicit aberrant proliferative and anti-apoptotic effects. These effects explain

our distinct dynamics of cellular responses to BMI-1 inactivation among normal and tumor cells,

and between patient-derived cells and DU145 cells, the latter are hormone insensitive cells

derived from metastasis and have activated PTEN but mutated p53.

The defects in Bmi-1 null mice are caused by inappropriate Ink4a/Arf expression [41]. The proteins $p16^{Ink4a}$ and $p19^{Arf}$, which induce cell-cycle arrest and apoptosis through activation of Rb and p53, respectively, are not expressed in normal tissue but induced upon oncogenic signaling [45]. The robust expression of BMI-1 in most PCa samples analyzed, the extreme sensitivity of PCa cells to BMI-1 inactivation vs normal RWPE1 cells, the upregulation of BMI-1 mRNA as an initial response to C-209 treatment, all suggest that PCa cells might have an oncogenic dependence over BMI-1 activity, possibly through increased transcriptional regulation, and similarly to the oncogenic addiction to Myc [46]. This dependence distinguishes TICs from normal stem cells and can be viewed as a survival mechanism, to maintain cancer cell viability, which could be exploited for targeted therapy. Overall, our data suggest that PCa cells are more sensitive to BMI-1 inhibition than normal cells, corroborating similar preferential sensitivity of PCa versus normal tissues to BET domain inhibitors [46]. We conclude that the identification of molecules targeting BMI-1, a self-renewal target involved in oncogenic addiction, may open new avenues to directly target TICs for PCa treatment while preserving normal stem cell populations.

Materials and Methods

Materials

Small molecule inhibitors were from PTC therapeutics, South Plainfield, NJ. Docetaxel (also called taxotere), doxorubicin, and methotrexate were from Rutgers Cancer Institute of New Jersey (CINJ) pharmacy. Cycloheximide was purchased from Cell Signaling. Collagen-I was bought from BD Biosciences, and NOD/SCID/IlRγ mice were from the Jackson laboratory.

Collagen adherence assay

Putative cancer stem-like cells, or TICs, were isolated by combining phenotypic analyses [3] with collagen adherence as described [6]. Briefly, tissue culture dishes were coated with 70 µg/ml of collagen-I for 1 hr at room temperature or overnight at 4°C. Subsequently, plates were washed with PBS and blocked in 0.3% BSA for 30 minutes. Cells were plated on collagen plates for 5 or 20 minutes. Next, cells adhering in 5 minutes and not adhering after 20 minutes were collected and used for further experiments.

Identification of BMI-1 post-transcriptional inhibitors

We have examined a small molecule library (PTC therapeutics) for post-transcriptional inhibitors of BMI-1 utilizing luciferase reporters encompassing the 5`UTR and 3`UTR of human BMI-1 [15]. Anti-BMI-1 antibody (Millipore, clone F6) was used for ELISA assays and western blotting (WB). The principal BMI-1's downstream target, mono-ubiquitinated (γ) histone H2A, was examined using a mouse monoclonal anti-ubiquityl-histone H2A antibody (clone E6C5) (Millipore). The selectivity of C-209 was further investigated by profiling it against both a library of purified protein kinase targets using the Z'-LYTE SelectScreen profiling activity assay

1 (Invitrogen) against 245 kinases at [ATP] Km and [C-209] (3μM), and a phosphatase profiler

2 assay with an IC_{50} profiler (Millipore). Both assays yielded <10% activity for C-209.

3

4 *Electrostatic potential and docking of C-209 to the human BMI-1 RNA*

5 All quantum mechanics calculations were performed using Gaussian 09. C-209 was geometry

6 optimized at the PM6 level using tight convergence. A single-point energy calculation at the

7 B3LYP/6-31G(d) level was performed and Merz-Kollman partial atomic charges were estimated

8 from the electrostatic potential. The reported energy is gas phase. The surface and contour plot

9 was prepared using the GaussView program. The electrostatic potential allowed us to build a

10 model for docking [47] of C-209 to the human BMI RNA. We used the UCSF DOCK program

11 (v6.7). The small molecule C-209 was built using the Spartan (Wavefunction, Inc) quantum

12 mechanics package and geometry optimized at the PM6 semi-empirical level. The Amber99SB

13 partial atomic charges were used on the RNA and AM1-BCC partial atomic charges were

14 calculated for C-209 within the UCSF Chimera molecular graphics package [47]. The interaction

15 energy scores (E_{int}) estimate the binding energy in the DOCK scoring of C-209 with BMI-1 RNA,

16 using guanine as a reference. DOCK scores, E_{vdw} (kcal/mol), E_{elec} (kcal/mol), and E_{int} (kcal/mol),

17 were generated using the following equation: $E_{int} = E_{vdw} + E_{elec}$. C-209 DOCK scores were E_{vdw}

18 (kcal/mol) -60.6, E_{elec} (kcal/mol) -5.2, and E_{int} (kcal/mol) -65.8, as compared to guanine scores of

19 E_{vdw} (kcal/mol) -36.4, E_{elec} (kcal/mol) -4.1, and E_{int} (kcal/mol) -40.5. The lower the energy score;

20 the more stable the complex contacts with the RNA due to complete fitting into the binding

21 pocket.

22

23

Patient-derived cell culture

Primary PCa cells were isolated from PCa specimens obtained at Rutgers CINJ in accordance with an Institutional Review Board (IRB)-approved protocol and upon informed consent from patients undergoing surgical resection. For isolation of prostate cells from surgical specimen, tissue was minced into small pieces and incubated with 1X collagenase (Sigma Aldrich) for 2 to 4 hours depending on the size of the tissue. After incubation, the dissociated pieces were strained with a 70µm filter to remove debris and the dissociated cells were washed with PBS at 250g for 2 minutes in order to eliminate fibroblasts. The recovered cells were cultured in prostate epithelial basal media (PrEBM, Lonza) for at least 14 days before being used for experiments at low passage numbers. Cells from immortalized PCa lines were maintained at low passage numbers in RPMI media (GIBCO), 10% fetal bovine serum, and 1% penicillin-streptomycin. TICs, obtained from DU145 cells after selection, were maintained in keratinocyte serum free medium (KSFM) supplemented with epidermal growth factor (EGF) and bovine pituitary extract (KSFM media) (All from Invitrogen). Protein analyses, flow cytometry, cell sorting, cell viability and survival assays, and cell migration assays are described in further details in the Supplementary Methods.

Spheroid forming assay

We have previously characterized spheroid forming (prostasphere) assays from multiple PCa cell lines and primary cells [6]. For prostasphere forming abilities, 2×10^3 cells/well were suspended in KSFM media and plated on 1% agarose coated plates. Every 3 days, half of the media was replaced and prostaspheres of >50 µm in diameter and consisting of >50 cells were counted on day14. Single cells from day-7 spheroids were used in secondary and tertiary spheroid assays. Colony forming abilities of PCa cells plated at 1×10^3 cells/well in six-well dishes coated with

1 1% agar were done as described [48]. The prostasphere and colony forming assays are described in

2 further details in the Supplementary Methods.

3

4 *Luciferase target assay*

5 pCDNA3.1+Luc Vector UTR, pCDNA3.1+Luc BMI-1 3'UTR, pCDNA3.1+ Luc BMI-1 5'UTR,

6 and pCDNA3.1+Luc BMI-1 5'&3'UTR were previously described [15]. Cells were transfected

7 using lipofectamine 2000 (Invitrogen). To normalize the transfection efficiency, cells were

8 transfected with pCMV-AcGFP1 at a ratio of 1/3 along with the UTR plasmids. These cells were

9 then visually counted for GFP$^+$ cells. After 19 hours, 5,000/well were seeded in a 96 well plate

10 and 6 hrs later, C-209 was added. At 24 hours post-treatment, cells were assayed for luciferase

11 activity using Steady-Glo system (Promega).

12

13 *Quantitative real-time PCR*

14 Total RNA was extracted using TRIzol Reagent (Life Technologies) and purification was

15 assessed with RNeasy plus Mini kit (Qiagen). cDNA was synthesized from 100 ng of total RNA

16 using SuperScript® VILO™ cDNA Synthesis Kit (Life Technologies) according to the

17 manufacturer's instruction. Synthesized cDNAs (10ng) were used as templates for real-time PCR

18 using EXPRESS SYBR® GreenER™ qPCR supermix. qPCR was performed in the StepOnePlus

19 real-time PCR system (Applied Biosystems). The geometric mean of the RNA Polymerase II

20 (RPOL2) housekeeping gene was used as an internal control. All amplicons were analyzed using

21 StepOne software V2.3 (Applied Biosystems). Primers used were: BMI-1 forward, 5`-

22 AACAATGGAATATGCCTTCTCTGC-3`;            BMI-1            reverse,            5`-

23 ACTGGGGACAATGAAATGTTTAGC-3`;    αENaC    forward,    5`-CCTCTGTCACGAT-

GGTCACCCTCC-3`; αENaC reverse, 5`-CAGCAGGTCAAAGACGAGCTCAG-3`; POLR2A

forward, 5`-GCACCACGTCCAATGACAT-3`; and POLR2A reverse, 5`-GTGCGGCTG

CTTCCATAA3`.

Labeling, transplantation and drug treatment of PCa grafts in zebrafish

Wild type EKK, Casper and *AB zebrafish (*Danio rerio*) were maintained following an approved

aquatic animal protocol. Adult fish were spawned and reared in conditioned water at 28.5°C on a

14-h-light 10-h-dark cycles. Embryos were staged as described (http://zfin.org). Quantum dots

(QDs) labeled human PCa cells were tracked in embryos and juvenile Casper fish as described [6].

Following initial imaging, transplanted embryos were maintained at 33°C for up to 12 days.

Juvenile zebrafish at 6-8 weeks of age were immune-suppressed with 10μg/ml dexamethazone for

2 days as described [49]. Xenografts were examined for QD fluorescence upon tumor formation

and treatment, and equal numbers of QD positive cells from pooled primary grafts were used for

injection into secondary recipients. Sections were examined for histological and IHC analyses and

compared to primary tissues as described [6], and further details are provided in the Supplementary

Methods.

Small molecular translation assay

Transcription and translation of BMI-1 *in vitro* was done utilizing the human BMI-1 cDNA.

Briefly, the full length 3.2 Kb fragment of the human BMI-1 cDNA (containing 5`UTR and

3`UTR) was subcloned into the BamHI site of pSK+ downstream of the T7 promoter. The

resulting pSK+-hBMI-1-cDNA vector was linearized with SacI, purified and utilized for TNT

coupled transcription/translation systems (Promega) following the manufacturer's instructions.

T7-mediated translation of mRNA (133 nM), after preincubation with or without 2µM C-209 for 60 min at 30ºC was performed in cell-free reticulocytes lysates. Aliquots of the transcribed products were run on an agarose gel to confirm equal transcription. The newly synthesized proteins were analyzed on SDS-polyacrylamide gel electrophoresis and probed for BMI-1 expression using the rabbit monoclonal anti-BMI-1 (D20B7) antibody (Cell signaling).

Treatment of mouse xenografts

Animal studies were performed according to Robert Wood Johnson Medical School IACUC protocol #I12-024-5. In order to differentiate tumoral from contaminating non-tumoral mouse cells, prior to mice injection, DU145 cells were infected with lentiviral vector encoding luciferase2/enhanced green fluorescent protein (Luc2/EGFP) that was generated as described [50]. Luc2/EGFP cells were suspended in 100 µl mixed 1:1 with matrigel (BD Biosciences) and injected subcutaneously (SC) into the left flank of six week-old NOD SCID IL-2Rnull (NSG) mice. After tumor formation, mice were randomized and SC administered with docetaxel 6 mg/kg once per week for 2 weeks, and C-209 at a dose of 60 mg/kg daily for twelve days. Tumor growth was evaluated with an electronic caliper before every administration, and measured every 3 days until day 30 and subsequently removed. Paraffin sections (5µm) were incubated with anti-Ki67 (Upstate-Millipore, Billerica, MA) and -CD44 (R&D Systems). To calculate retention of tumor-seeding capacity, tumor xenografts were dissociated following treatments, and recovered cells were sorted for EGFP. Equal numbers of EGFP positive cells were next re-injected into secondary recipients.

Statistical analysis

All statistical analyses were performed using GraphPad Prism 6 (GraphPad Software Inc). Data are presented as mean ± standard deviation (S.D.). Statistical significance was determined by student's t-test or ANOVA (one-way or two-way) with Bonferroni post-hoc test. Mann-Whitney U test was used to compare the differences in xenograft tumor volumes between two groups. A P value <0.05 is represented by a single asterisk, a P value <0.01 is represented by a double asterisk, three asterisks indicate P<0.001 while four asterisks indicate P<0.0001.

References

1   Siegel RL, Miller KD, Jemal A. Cancer statistics, 2015. CA Cancer J Clin 2015; **65** (1):5-29.

2   Attard G, Parker C, Eeles RA *et al.* Prostate cancer. Lancet 2015.

3   Collins AT, Berry PA, Hyde C, Stower MJ, Maitland NJ. Prospective identification of tumorigenic prostate cancer stem cells. Cancer Res 2005; **65** (23):10946-10951.

4   Goldstein AS, Lawson DA, Cheng D *et al.* Trop2 identifies a subpopulation of murine and human prostate basal cells with stem cell characteristics. Proc Natl Acad Sci U S A 2008; **105** (52):20882-20887.

5   Toivanen R, Berman DM, Wang H *et al.* Brief report: a bioassay to identify primary human prostate cancer repopulating cells. Stem Cells 2011; **29** (8):1310-1314.

6   Bansal N, Davis S, Tereshchenko I *et al.* Enrichment of human prostate cancer cells with tumor initiating properties in mouse and zebrafish xenografts by differential adhesion. Prostate 2014; **74** (2):187-200.

7   Qin J, Liu X, Laffin B *et al.* The PSA(-/lo) prostate cancer cell population harbors self-renewing long-term tumor-propagating cells that resist castration. Cell Stem Cell 2012; **10** (5):556-569.

8   Hoogland AM, Verhoef EI, Roobol MJ *et al.* Validation of stem cell markers in clinical prostate cancer: alpha6-integrin is predictive for non-aggressive disease. Prostate 2014; **74** (5):488-496.

9   Kreso A, Dick JE. Evolution of the cancer stem cell model. Cell Stem Cell 2014; **14** (3):275-291.

10   Park IK, Qian D, Kiel M *et al.* Bmi-1 is required for maintenance of adult self-renewing haematopoietic stem cells. Nature 2003; **423** (6937):302-305.

11   Lukacs RU, Memarzadeh S, Wu H, Witte ON. Bmi-1 is a crucial regulator of prostate stem cell self-renewal and malignant transformation. Cell Stem Cell 2010; **7** (6):682-693.

12   van Leenders GJ, Dukers D, Hessels D *et al.* Polycomb-group oncogenes EZH2, BMI1, and RING1 are overexpressed in prostate cancer with adverse pathologic and clinical features. Eur Urol 2007; **52** (2):455-463.

13   Glinsky GV. Death-from-cancer signatures and stem cell contribution to metastatic cancer. Cell Cycle 2005; **4** (9):1171-1175.

14   Visvader JE, Lindeman GJ. Cancer stem cells in solid tumours: accumulating evidence and unresolved questions. Nat Rev Cancer 2008; **8** (10):755-768.

15   Cao L, Bombard J, Cintron K *et al.* BMI1 as a novel target for drug discovery in cancer. J Cell Biochem 2011; **112** (10):2729-2741.

16   Peltz SW, Welch EM, Trotta CR, Davis T, Jacobson A. Targeting post-transcriptional control for drug discovery. RNA Biol 2009; **6** (3):329-334.

17   Meng S, Luo M, Sun H *et al.* Identification and characterization of Bmi-1-responding element within the human p16 promoter. J Biol Chem; **285** (43):33219-33229.

18   Dimri M, Bommi PV, Sahasrabuddhe AA, Khandekar JD, Dimri GP. Dietary omega-3 polyunsaturated fatty acids suppress expression of EZH2 in breast cancer cells. Carcinogenesis 2009; **31** (3):489-495.

19   Chagraoui J, Hebert J, Girard S, Sauvageau G. An anticlastogenic function for the Polycomb Group gene Bmi1. Proc Natl Acad Sci U S A 2011; **108** (13):5284-5289.

20   Franken NA, Rodermond HM, Stap J, Haveman J, van Bree C. Clonogenic assay of cells in vitro. Nat Protoc 2006; **1** (5):2315-2319.

21   Obrig TG, Culp WJ, McKeehan WL, Hardesty B. The mechanism by which cycloheximide and related glutarimide antibiotics inhibit peptide synthesis on reticulocyte ribosomes. J Biol Chem 1971; **246** (1):174-181.

22   Sipes NS, Padilla S, Knudsen TB. Zebrafish: as an integrative model for twenty-first century toxicity testing. Birth Defects Res C Embryo Today 2011; **93** (3):256-267.

23   Migneault F, Boncoeur E, Morneau F *et al.* Cycloheximide and lipopolysaccharide downregulate alphaENaC mRNA via different mechanisms in alveolar epithelial cells. Am J Physiol Lung Cell Mol Physiol 2013; **305** (10):L747-755.

24   Nacerddine K, Beaudry JB, Ginjala V *et al.* Akt-mediated phosphorylation of Bmi1 modulates its oncogenic potential, E3 ligase activity, and DNA damage repair activity in mouse prostate cancer. J Clin Invest 2012; **122** (5):1920-1932.

25   Alkema MJ, Bronk M, Verhoeven E *et al.* Identification of Bmi1-interacting proteins as constituents of a multimeric mammalian polycomb complex. Genes Dev 1997; **11** (2):226-240.

26   Sabaawy HE. Genetic Heterogeneity and Clonal Evolution of Tumor Cells and their Impact on Precision Cancer Medicine. J Leuk (Los Angel) 2014; **1** (4):1000124.

27   Berezovska OP, Glinskii AB, Yang Z *et al.* Essential role for activation of the Polycomb group (PcG) protein chromatin silencing pathway in metastatic prostate cancer. Cell Cycle 2006; **5** (16):1886-1901.

28   Risbridger GP, Taylor RA. Minireview: regulation of prostatic stem cells by stromal niche in health and disease. Endocrinology 2008; **149** (9):4303-4306.

29   Chaux A, Albadine R, Toubaji A *et al.* Immunohistochemistry for ERG expression as a surrogate for TMPRSS2-ERG fusion detection in prostatic adenocarcinomas. Am J Surg Pathol 2011; **35** (7):1014-1020.

30   White R, Rose K, Zon L. Zebrafish cancer: the state of the art and the path forward. Nat Rev Cancer 2013; **13** (9):624-636.

31   Chen J, Li Y, Yu TS *et al.* A restricted cell population propagates glioblastoma growth after chemotherapy. Nature 2012; **488** (7412):522-526.

32   Schepers AG, Snippert HJ, Stange DE *et al.* Lineage tracing reveals Lgr5+ stem cell activity in mouse intestinal adenomas. Science 2012; **337** (6095):730-735.

33   Reya T, Morrison SJ, Clarke MF, Weissman IL. Stem cells, cancer, and cancer stem cells. Nature 2001; **414** (6859):105-111.

34   Liu S, Dontu G, Mantle ID *et al.* Hedgehog signaling and Bmi-1 regulate self-renewal of normal and malignant human mammary stem cells. Cancer Res 2006; **66** (12):6063-6071.

35   Bisson I, Prowse DM. WNT signaling regulates self-renewal and differentiation of prostate cancer cells with stem cell characteristics. Cell Res 2009; **19** (6):683-697.

36   Mehta M, Khan A, Danish S, Haffty BG, Sabaawy HE. Radiosensitization of Primary Human Glioblastoma Stem-like Cells with Low-Dose AKT Inhibition. Mol Cancer Ther 2015; **14** (5):1171-1180.

37   Guzman-Ramirez N, Voller M, Wetterwald A *et al.* In vitro propagation and characterization of neoplastic stem/progenitor-like cells from human prostate cancer tissue. Prostate 2009; **69** (15):1683-1693.

38   Rizo A, Dontje B, Vellenga E, de Haan G, Schuringa JJ. Long-term maintenance of human hematopoietic stem/progenitor cells by expression of BMI1. Blood 2008; **111** (5):2621-2630.

39   Yang MH, Hsu DS, Wang HW *et al.* Bmi1 is essential in Twist1-induced epithelial-mesenchymal transition. Nat Cell Biol 2010; **12** (10):982-992.

40   Meng S, Luo M, Sun H *et al.* Identification and characterization of Bmi-1-responding element within the human p16 promoter. J Biol Chem 2010; **285** (43):33219-33229.

41   Molofsky AV, He S, Bydon M, Morrison SJ, Pardal R. Bmi-1 promotes neural stem cell self-renewal and neural development but not mouse growth and survival by repressing the p16Ink4a and p19Arf senescence pathways. Genes Dev 2005; **19** (12):1432-1437.

42   Wachter A, Tunc-Ozdemir M, Grove BC *et al.* Riboswitch control of gene expression in plants by splicing and alternative 3' end processing of mRNAs. Plant Cell 2007; **19** (11):3437-3450.

43   Barbieri CE, Bangma CH, Bjartell A *et al.* The mutational landscape of prostate cancer. Eur Urol 2013; **64** (4):567-576.

44   Magee JA, Piskounova E, Morrison SJ. Cancer stem cells: impact, heterogeneity, and uncertainty. Cancer Cell 2012; **21** (3):283-296.

45   Serrano M, Lee H, Chin L *et al.* Role of the INK4a locus in tumor suppression and cell mortality. Cell 1996; **85** (1):27-37.

46   Asangani IA, Dommeti VL, Wang X *et al.* Therapeutic targeting of BET bromodomain proteins in castration-resistant prostate cancer. Nature 2014; **510** (7504):278-282.

47   Pettersen EF, Goddard TD, Huang CC *et al.* UCSF Chimera--a visualization system for exploratory research and analysis. J Comput Chem 2004; **25** (13):1605-1612.

48   Patrawala L, Calhoun T, Schneider-Broussard R *et al.* Side population is enriched in tumorigenic, stem-like cancer cells, whereas ABCG2+ and ABCG2- cancer cells are similarly tumorigenic. Cancer Res 2005; **65** (14):6207-6219.

49   Sabaawy HE, Azuma M, Embree LJ *et al.* TEL-AML1 transgenic zebrafish model of precursor B cell acute lymphoblastic leukemia. Proc Natl Acad Sci U S A 2006; **103** (41):15166-15171.

50   Kokorina NA, Granier CJ, Zakharkin SO *et al.* PDCD2 knockdown inhibits erythroid but not megakaryocytic lineage differentiation of human hematopoietic stem/progenitor cells. Exp Hematol 2012; **40** (12):1028-1042 e1023.

1 **Table S1** Primary prostate cancer patient characteristics.

2

Primary prostate cancer	Age	Type	Grade	pTNM	Gleason	BMI-1 expression by IHC
						H-score
15728	62	Adc	3	pT2c	3 + 3	120
17148	52	Adc	3	pT2c	3 + 3	150
17761	57	Adc	3	pT2c	3 + 3	ND
19803	55	Adc	3	pT2c	3 + 3	70
24126	53	Adc	4	pT3a	3 + 3	190
40181	60	Adc	4	pT3a	3 + 4	ND
25185	67	Adc	3	pT2c	3 + 3	200
25315	66	Adc	4	pT3a	3 + 4	150
26136	67	Adc	3	pT3b	4 + 5	220
25854	55	Adc	4	pT3b	4 + 5	190
28838	65	Adc	4	pT3b	4 + 4	160
28864	68	Adc	3	pT3b	3 + 4	210
28869	67	Adc	4	pT2c	4 + 4	200
29032	68	Adc	4	pT3b	4 + 5	210
29084	58	Adc	3	pT2c	3 + 3	ND
29092	71	Adc	4	pT3b	4 + 4	210
29110	69	Adc	4	pT3c	4 + 5	130
29663	50	mAdc	4	pT3b	4 + 5	250
29834	44	Adc	3	pT2c	3 + 4	160
29990	63	Adc	4	pT3a	4 + 3	200
33020	45	Adc	3	pT2c	3 + 4	165
33106	64	mAdc	5	pT3b	5 + 4	180
33072	48	Adc	4	pT3a	4 + 3	200
33120	47	Adc	3	pT2c	3 + 4	200

3

4 Table shows the de-identified number of each patient, age, prostate cancer type (Adc, adenocarcinoma,
5 mAdc, metastatic adenocarcinoma), histological grade, pathological staging based on the pTNM
6 classification, where pT2c indicates bilateral prostate disease, and total Gleason scores. BMI-1

expression is assessed as the extent of nuclear immunoreactivity by IHC and indicated as an H score. The H score is obtained using the following formula: H-Score = (% at 0) * 0 + (% at 1+) * 1 + (% at 2+) * 2 + (% at 3+) * 3. Scoring was determined as (3 X percentage of BMI-1 strongly staining nuclei + 2 X percentage of BMI-1 moderately staining nuclei + 1 X percentage of BMI-1 weakly staining nuclei), giving a range of 0 to 300. Weak cytoplasmic and/or stromal staining was seen in a few sections and was not considered in the score. BMI-1 staining in multiple sections from the same patient's tumor displayed marked heterogeneity. ND, not determined due to insufficient tissue material.

1

2 **Figure legends**

3 **Figure 1** Assessment of BMI-1 in PCa TICs isolated by combined adherence and phenotypic

4 assays. (**A**) Diagram depicting the combined time of adherence and phenotypic assay used to

5 isolate TICs from DU145 cells and assess BMI-1 expression in different subpopulations of cells.

6 (**B**) Flow cytometric analyses. (**C**) Percentage of cells identified by flow cytometry to express the

7 TIC phenotype. (**D**) Q-PCR analyses of BMI-1 in subpopulations of DU145 cells. Relative

8 mRNA BMI-1 level in total, $CD49b^{hi}CD29^{hi}CD44^{hi}$ (high) and $CD49b^{low}CD29^{low}CD44^{low}$ (low)

9 DU145 cells. (**E**) Western blot analysis showing BMI-1 expression levels between total,

10 $CD49b^{hi}CD29^{hi}CD44^{hi}$ and $CD49b^{low}CD29^{low}CD44^{low}$ DU145 cells. (**F**) Quantitation of BMI-1

11 expression levels from 6 independent experiments. Anti-actin was used as a loading control. (**G**)

12 Fold adhesion of rapidly adherent $CD49b^{hi}CD29^{hi}CD44^{hi}$ cells assessed over total DU145

13 control (Sh-Scr) and DU145 BMI-1-depleted (Sh-BMI-1) cells. Results are shown as mean $\pm$

14 S.D. of three independent experiments. **P-value <0.01, ***P-value <0.001.

15

16 **Figure 2** BMI-1 inhibition reduces TIC number and interferes with self-renewal capacity *in*

17 *vitro*. (**A**) Chemical core structure of small molecules targeting BMI-1. Ar_1 is aryl or

18 heterocyclyl; Ar_2 is heterocyclyl; R^1 is hydrogen; R^2 is hydrogen; and R^3 is C1-8 alkyl. (**B**) Fold

19 adhesion of rapidly adherent $CD49b^{hi}CD29^{hi}CD44^{hi}$ cells evaluated upon treatment of total

20 DU145 with inhibitors targeting BMI-1 for 72hrs. (**C**) IC_{50s} of compounds C-209-211 assessed in

21 DU145 cells through an ELISA assay. (**D**) Western blot analysis showing BMI-1 and EZH2

22 expression levels in DU145 cells treated for 72 hours with C-209, C-210 and C-211 at 1x and 2x

23 of the IC_{50} concentrations. GAPDH levels were used as controls. (**E**) Representative

24 cytofluorimetric analysis showing reduction of $CD49b^{hi}CD29^{hi}CD44^{hi}$ prostate TICs upon C-209

treatment. DU145 cells were treated with C-209 (2μM) for 72 hours. These cells were then subjected to time-of-adherence assay, stained, and examined using flow cytometry and Cell Quest software. (**F**) Graphical representation showing impaired percentage of CD49b^{hi}CD29^{hi}CD44^{hi} TIC phenotype in DU145, PC3 and CWR22 cells following C-209 treatment. Data are displayed as mean ± S.D. of three independent experiments. (**G**) Effects of BMI-1 post-transcriptional inhibitors vs. the non-specific protein translation inhibitor cycloheximide (CHX), or the chemotherapeutics methotrexate (MTX) and doxorubicin on secondary (left) and tertiary (right) prostate spheroids formation. Treatments that were statistically significant were indicated as $^{*}p$ <0.05 and $^{**}p$<0.01, compared to untreated.

Figure 3 Modulation of BMI-1 post-transcriptional regulation by C-209. (**A**) Chemical structure of C-209. (**B**) The electrostatic potential of C-209 mapped to electron density surface. At an IC$_{50}$ of 2μM, the electrostatic potential E(RB3LYP) = -1423.42386733 au and dipole moment = 9.4906 Debye. (**C**) Docking of C-209 to the human BMI-1 RNA. View of C-209 (space filling model colored magenta) within the binding pocket of the BMI-1 5`UTR model (ribbon). Illustration was created using the Pymol software package. (**D**) Schematic diagram of the luciferase (Luc) constructs used. The base pair (bp) length of the human BMI-1 5` and 3`UTRs are displayed (from full length cDNA # L.13689.1). Boxes are drawn not to scale. (**E**) DU145 cells containing Luc flanked by control UTRs or BMI-1 5' or 3' UTR regions were treated for 24 hrs with 2μM C-209 and compared against untreated and DMSO controls. IRES-containing BMI-1 5`UTR and 3`UTR were shown to regulate Luc expression [15]. The 5`UTR reduced Luc expression, while when combined with the 3`UTR reversed the Luc expression reducing effects demonstrating the regulatory effects of the BMI-1 5`UTR and 3`UTR. Treatment with 2μM C-

209 reversed the expression suppressing effects of the 5`UTR, and resulted in reduced Luc expression opposing the effects of the 3`UTR. Data plotted represent three independent experiments. (**F**) Timed modulation of BMI-1 protein expression upon C-209 (2μM) exposure. (**G**) Percentage of inhibition of Luc reporter cells with either control (Cont.) vs. BMI-1 5` and 3`UTR cells following C-209 (0.0195-20μM) treatments for 72hrs. (**H**) Histogram depicting relative mRNA transcript expression of BMI-1 and αENaC from DU145 cells treated with C-209 2μM for 24 and 72hrs and compared to the effects of treatment with CHX 20μg/ml for 24 hr. Values were normalized over POLR2A housekeeping control. (**I**) Top, Western blot (WB) analysis for BMI-1 expression in CHX (1-50 μg/ml) treated cells. Bottom, quantitation of relative BMI-1 protein expression upon treatments with CHX and C-209. (**J**) Selective effects of C-209 on BMI-1 mRNA translation in cell-free extracts. Top, WB analysis of translated full-length BMI-1 RNA (complete cDNA including BMI-1 5` and 3`UTRs) in *in vitro* transcription/translation (TNT) assays in eukaryotic cell-free rabbit reticulocytes. A cellular lysate in the left most lane was used as a positive control to determine the BMI-1 migrated band on the polyacrylamide gel at a position of ~37 KDa. Bottom, quantitation of normalized translated BMI-1 from BMI-1 cDNA pretreated or not with 2μM C-209 for one hour compared to control. (**K**) BMI-1 expression in vector-transduced (Sh-Scr), BMI-1-overexpressing (EGFP-BMI-1) and BMI-1-depleted (shBMI-1) DU145 cells. **L**, Cell viability evaluated in vector-transduced (Sh-Scr), BMI-1-overexpressing (EGFP-BMI-1) and BMI-1-depleted (shBMI-1) DU145 cells following C-209 (0.0195-20μM) treatments for 72hrs.

Figure 4 Antitumor activities of C-209 against patient-derived TICs. (**A**) BMI-1 expression levels assessed in normal (N) and tumoral (T) patient-derived samples before and after C-209

1   (2μM) treatment for 72hrs. (**B**) Antitumor activity of C-209 in DU145 and primary PCa cells.

2   Percentage of survival was evaluated by MTS assay. (**C**) Representative cytofluorimetric

3   analysis (left panel) and graphical plotting (right panel) of TIC modulation in primary patient-

4   derived cells untreated and treated with C-209 (2μM) and docetaxel (2.5nM) for 72h. (**D-F**)

5   Primary PCa cell survival, clonogenicity and motility assessed after pre-treatment with DMSO,

6   C-209 (2μM) or docetaxel (2.5nM) for 96hrs. Data are displayed as mean percentage ± S.D.

7   Single independent experiments were performed with four to eight distinct patient-derived cells.

8    $^*p < 0.05$, $^{**}p < 0.01$ and $^{***}p < 0.001$.

9

10   **Figure 5** Xenografts of human primary PCa cells in embryonic zebrafish. (**A**) Schematic

11   illustration of the experimental procedure for the use of zebrafish PCa xenografts to identify

12   small molecules targeting BMI-1 *in vivo*. (**B-D**) Histological sections from prostate cancer

13   patient #24126 stained with H&E. Notice the morphology of the cells in **D** (arrow). (**E-G**)

14   Formalin fixed paraffin embedded (FFPE) sections from a representative primary PCa tissue

15   used that are stained with dual IHC or single IHC for Erg (in brown) or AMACR (in pink)

16   showing identical expression pattern of both tumor markers (arrows). (**H-K**) Histological

17   sections from a representative zebrafish xenograft at 8 dpt demonstrating tumor growth (arrow in

18   **I**). (**J-K**) higher magnification of the tumor area in **I**. Notice that the morphology of the cells in

19   **K** (arrows) is identical to the primary tissue sample in **D**. (**L-O**) IHC staining of the section in **M**

20   showing expression of PSA in cells (arrow) of primary PCa fish xenografts. Scale bars are 250

21   μm in **B**, **E**, **H**, and 10 μm in **D**, **F**, **G**, **K** and **O**.

22

Figure 6 Treatment effects of C-209 on zebrafish xenografts. (**A**) Representative images of vehicle-, and QD-labeled primary CD49b^{hi}CD29^{hi}CD44^{hi} engrafted cells. Images are overlays of bright, GFP and red 605 fluorescent images at 4 days post-transplantation (dpt). (**B**) Anti-tumor activity of C-209. Reduction in tumor size monitored with reduced QD fluorescence (blue arrows). (**C**) Anti-tumor activity of C-209 (2μM) against xenografts derived from either parental cells (yellow) or the TIC fraction (orange) from three primary samples. The graph demonstrates responses to C-209 as a percentage of total treated xenografts (n=25 xenograft per cell fraction per patient). (**D**) Evaluation of tumor area variation calculated as fluorescence intensity of untreated and treated xenografts with C-209 (2μM). Data are presented as mean value ± S.D. (**E**) Tumorigenic capacity of primary PCa TICs in zebrafish xenografts. Cells, pre-treated with C-209 (2μM) or docetaxel (2.5nM), were washed after 4 days, plated in fresh media for 3 days and subsequently injected in equal number into adult zebrafish. Data are displayed as mean percentage ± S.D. from four distinct patients (#29663, #29834, #29084 and #29990). (**F**) The graph displays the percentage ± S.D. of Ki67 positive cells in DMSO (control), C-209 (2μM) or docetaxel (2.5nM) treated-cells. (**G**) Strategy employed to determine inhibition of tumor initiation potential of remaining treated cells in secondary xenografts. TICs of patient samples #40181, #26136, and #25854 were transplanted to generate primary xenografts (1º). Diagram on the right demonstrates primary graft take rates. Xenografts were treated (TRT) with either DMSO or C-209 at 2μM for 72 hours, tumor areas were dissected, pooled, and TICs were sorted and injected into secondary recipients. Treatment with C-209 significantly reduced the rates of secondary xenografts (2º). (**H-I**) BMI-1 expression (arrows) in sections of primary and metastatic colonies derived from TIC zebrafish grafts. The numbers of BMI-1^{+} cells were

1 derived from analyses of primary and metastatic xenografts (n= 9 each). Scale bars are 250 μm

2 in **B** and 50 μm in **H.**

3

4 **Figure 7** *In vivo* pharmacological targeting of BMI-1 in mouse PCa xenografts. (**A**) Strategy for

5 examining the antitumor activity of C-209 in serial mouse xenografts and clonogenic

6 repopulation assays of treated cells. (**B**) Growth rate of mouse xenografts generated after

7 subcutaneous (SC) injection of CD49b^{hi}CD29^{hi}CD44^{hi} Luc2EGFP cells. Mice were randomized

8 and administered daily with 60 mg/kg/day of C-209 for ten days and docetaxel 6mg/kg once a

9 week for two consecutive weeks. Results are mean ± S.D. of six independent experiments.

10 Comparison of tumor volumes between the three groups was determined by two-way ANOVA

11 with Bonferroni post-hoc test. Graph indicates significance of Docetaxel *vs.* Control at day 30

12 (**$p<0.01$) and C-209 *vs.* Control at day 30 (****$p<0.0001$). There was a trend towards

13 significance ($p=0.08$) when comparing tumor volumes in xenograft treated with C-209 *vs.*

14 Docetaxel at day 30 using Mann-Whitney U test. At the earlier days 20 and 25, Docetaxel was

15 not significantly different than Control, while C-209 was; C-209 *vs.* Control at day 20 (*$p<0.05$);

16 C-209 *vs.* Control at day 25 (**$p<0.01$). Red arrow indicates treatment discontinuation. In each

17 experiments, n=8/group. (**C**) Representative H&E staining of mouse xenograft sections showing

18 histological effects of treatments. (**D**) Intratumor IHC revealed reduced nuclear BMI-1 (brown)

19 and surface CD44 (red) staining upon treatment with C-209. (**E**) Quantitation of Ki67 positive

20 cells in sections from treated xenografts. (***$p<0.001$). (**F**) Colony-forming ability assay

21 performed on freshly dissociated and EGFP sorted xenograft-cells. Average number of

22 colonies/plate for each treatment mean ± S.D. of two independent experiments with 12

23 wells/condition is reported. *$p<0.05$, ***$p<0.001$ (**G**) Tumor initiation potential in serial grafting

1   in secondary mouse xenografts of cells dissociated from treated primary mouse xenografts (n=8
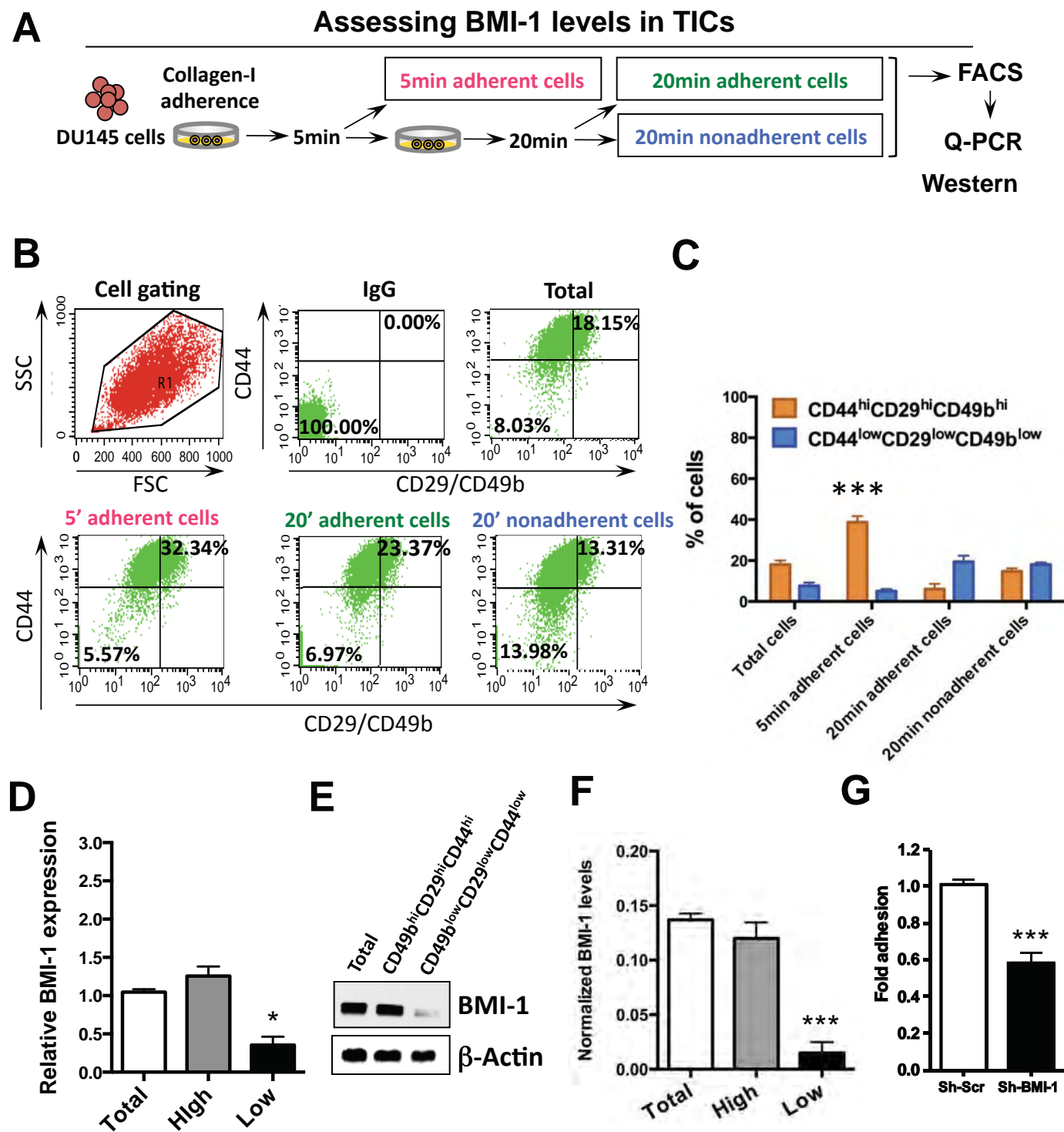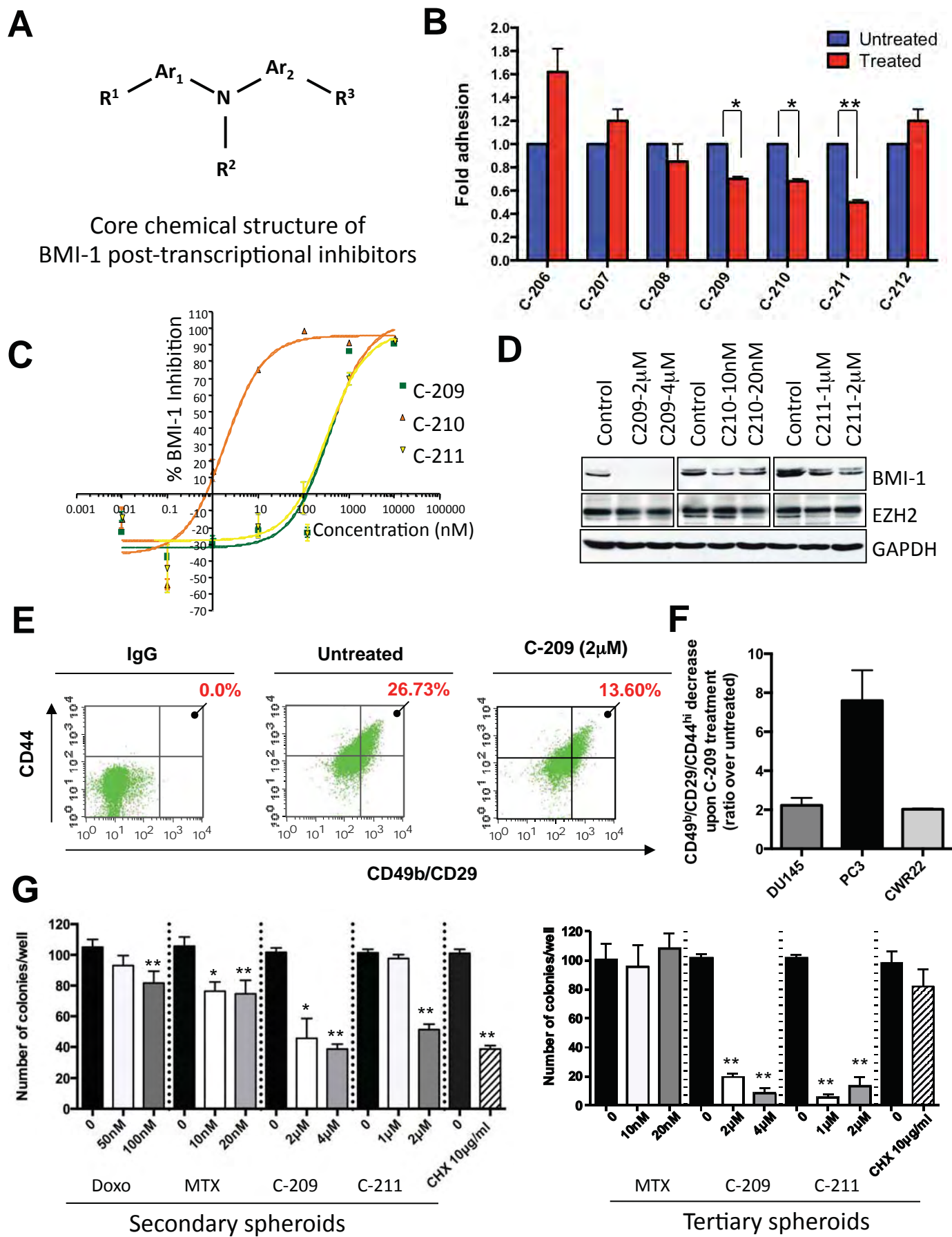
2   mice /group, *p<0.01).

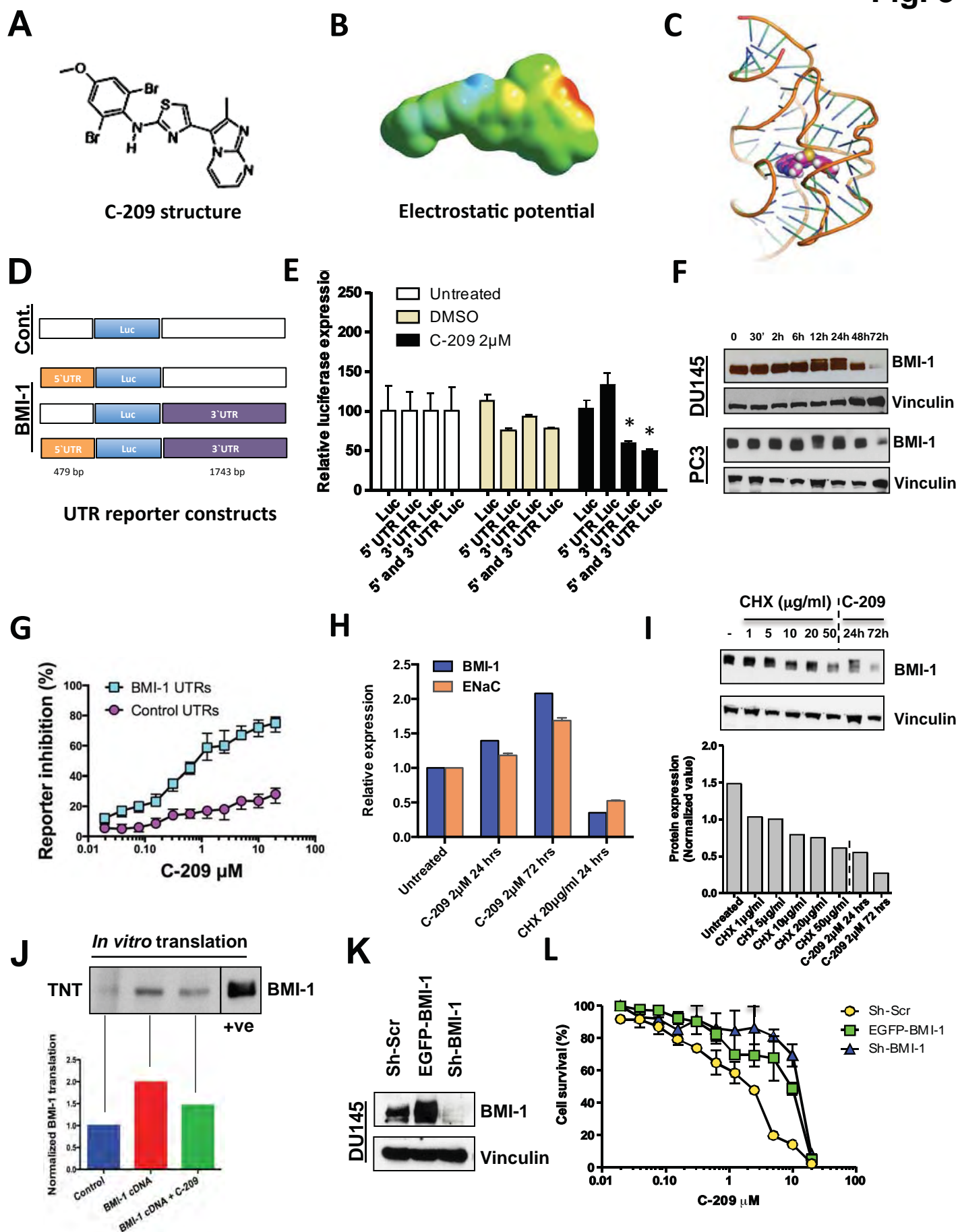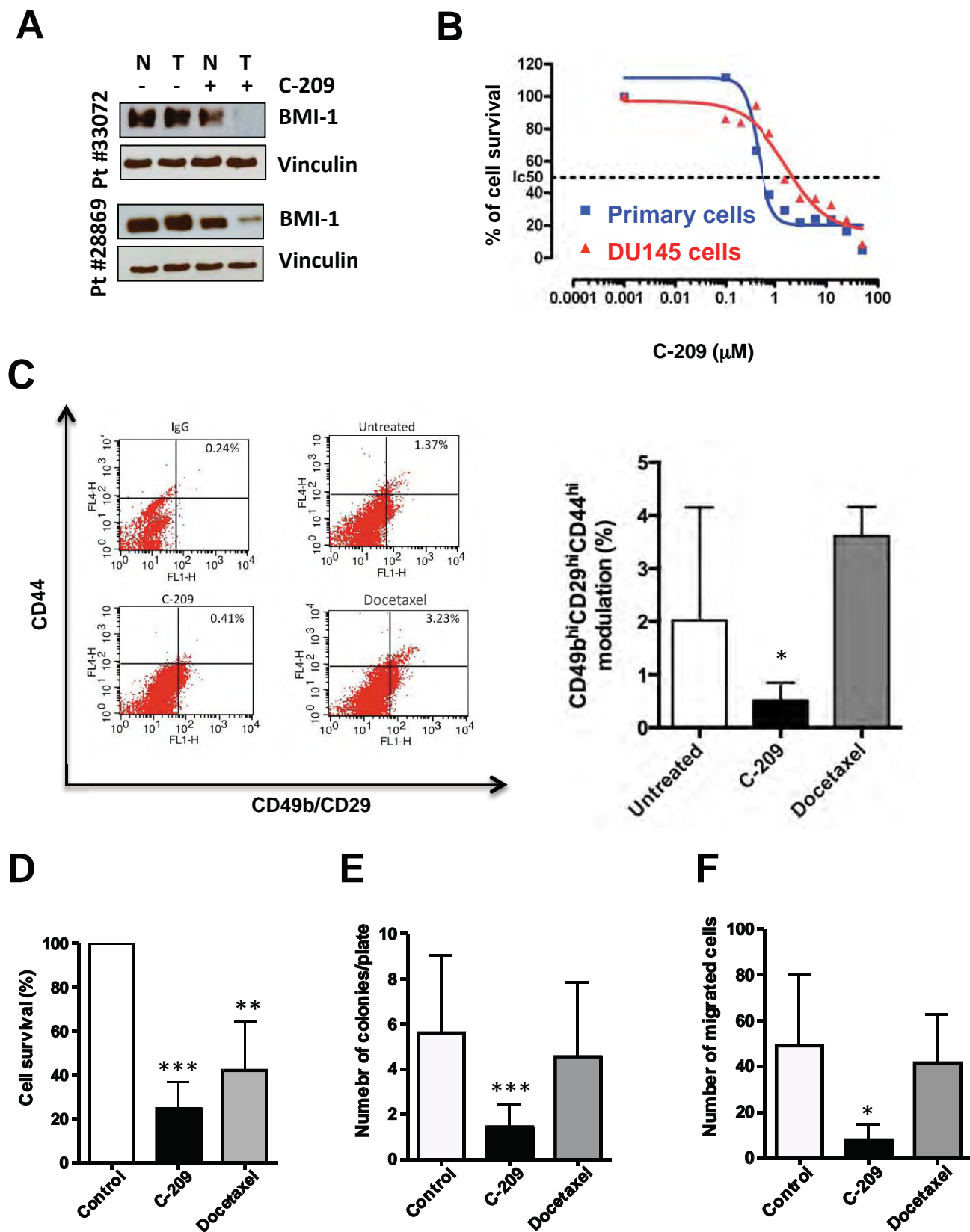**Fig. 1**

A Assessing BMI-1 levels in TICs

B

C

D

E

F

G

Fig. 2

A

R¹—Ar₁—N—Ar₂—R³ with R² below N

Core chemical structure of
BMI-1 post-transcriptional inhibitors

B Fold adhesion — Untreated (blue) / Treated (red), C-206 through C-212
* (C-209), * (C-210), ** (C-211)

C % BMI-1 Inhibition vs Concentration (nM): C-209, C-210, C-211

D Western blot: Control, C209-2µM, C209-4µM, Control, C210-10nM, C210-20nM, Control, C211-1µM, C211-2µM — BMI-1, EZH2, GAPDH

E CD44 vs CD49b/CD29: IgG 0.0%, Untreated 26.73%, C-209 (2µM) 13.60%

F CD49b/CD29/CD44^hi decrease upon C-209 treatment (ratio over untreated): DU145, PC3, CWR22

G Secondary spheroids: Number of colonies/well — Doxo (0, 50nM, 100nM), MTX (0, 10nM, 20nM), C-209 (0, 2µM, 4µM), C-211 (0, 1µM, 2µM), CHX 10µg/ml

Tertiary spheroids: Number of colonies/well — MTX (0, 10nM, 20nM), C-209 (0, 2µM, 4µM), C-211 (0, 1µM, 2µM), CHX 10µg/ml

Fig. 3

A C-209 structure

B Electrostatic potential

C

D UTR reporter constructs

E
Untreated
DMSO
C-209 2µM

F
0 30' 2h 6h 12h 24h 48h 72h

DU145 BMI-1
Vinculin

PC3 BMI-1
Vinculin

G
BMI-1 UTRs
Control UTRs

H
BMI-1
ENaC

I
CHX (µg/ml) C-209
- 1 5 10 20 50 24h 72h

BMI-1
Vinculin

J *In vitro* translation
TNT BMI-1
+ve

K
Sh-Scr
EGFP-BMI-1
Sh-BMI-1

DU145 BMI-1
Vinculin

L
Sh-Scr
EGFP-BMI-1
Sh-BMI-1

Fig. 4

A

	N	T	N	T	
	−	−	+	+	C-209

Pt #33072: BMI-1, Vinculin

Pt #28869: BMI-1, Vinculin

B

% of cell survival vs C-209 (µM)
Ic50
■ Primary cells
▲ DU145 cells

C

CD44 vs CD49b/CD29

IgG 0.24%
Untreated 1.37%
C-209 0.41%
Docetaxel 3.23%

CD49b^hi CD29^hi CD44^hi modulation (%)
Untreated, C-209 *, Docetaxel

D

Cell survival (%)
Control, C-209 ***, Docetaxel **

E

Numebr of colonies/plate
Control, C-209 ***, Docetaxel

F

Number of migrated cells
Control, C-209 *, Docetaxel

Fig. 5

A

Strategy to target BMI-1 in zebrafish xenografts of prostate cancer TICs

Collagen-I adherence → 5 min adherent → CD49b^{hi}CD29^{hi}CD44^{hi}

Colonies/spheres

Migration

20 min non-adherent → CD49b^{low}CD29^{low}CD44^{low}

B 1^{ry} PCa   H&E

C

D

E Erg/AMACR

F Erg

G AMACR

H 1^{ry} PCa graft   H&E

I

J

K

L 1^{ry} PCa graft   PSA

M

N

O

Fig. 6

Fig. 7

A Targeting BMI-1 in mouse xenografts of prostate cancer TICs

B

C

D

E

F

G

**BMI-1 targeting interferes with patient-derived tumor-initiating cell survival and tumor growth in prostate cance**r   Nitu Bansal, Monica Bartucci, Shamila Yusuff, Stephani Davis, Kathleen Flaherty, Eric Huselid, Michele Patrizii, Daniel Jones, Liangxian Cao, Nadiya Sydorenko, Young-Choon Moon, Hua Zhong, Daniel J. Medina, John Kerrigan, Mark N. Stein, Isaac Y. Kim, Thomas W. Davis, Robert S. DiPaola, Joseph R. Bertino, Hatem E. Sabaawy
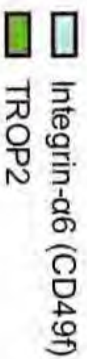
Supplementary figures
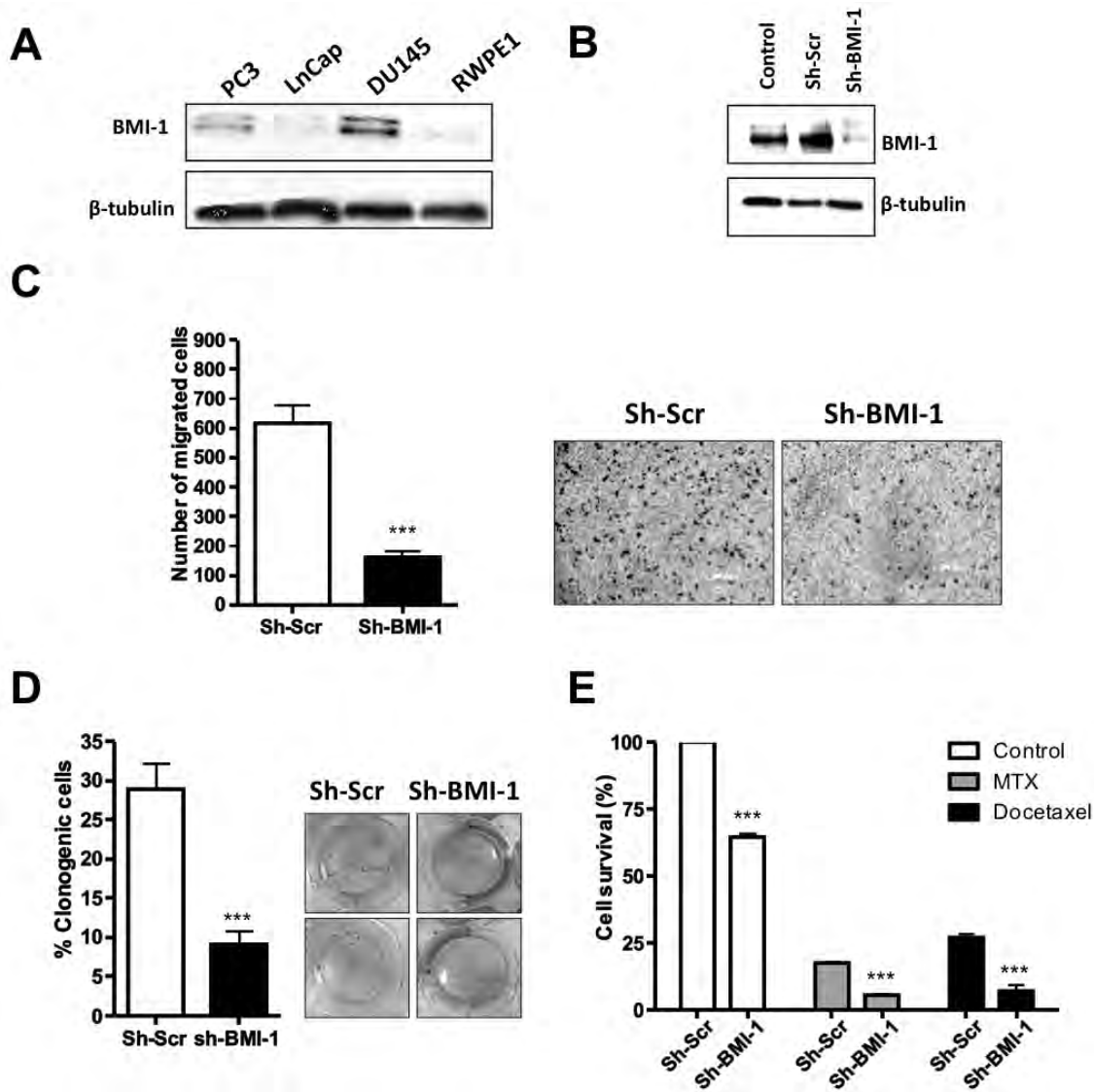
Supplementary Figure S1 Functional role(s) of BMI-1 in PCa. (**A**) Western Blot analysis for BMI-1 expression in prostate cancer cell lines (PC3, LNCap, and DU145), and in immortalized normal prostate epithelial cells (RWPE-1). (**B**) Western blot analysis for BMI-1 expression in cell lysates from untransduced DU145, control vector-transduced (Sh-Scr) and BMI-1-depleted (shBMI-1) cells. β-tubulin was used to assess equal loading. (**C**) Left: Graph showing the number of migrated cells in standard growth conditions. For the migration assay, 20.,000 DU145 Sh-Scr and sh-BMI-1 cells were plated in modified Boyden chambers. Migrated cells were stained with Comassie Blue and counted under the microscope after 96h (Scale bars 200μm). A representative image is shown (right panel). Graph is showing the outcome of three independent experiments. (**D**) Percentage of clonogenic cells upon BMI-1 knockdown compared to sh-Scr control. Images on the right demonstrate colonies stained with crystal violet. (**E**) Percentage of cell survival upon combined knockdown of BMI-1 and treatment with chemotherapeutic agent methotrexate (MTX, 10nM) or docetaxel (2.5 nM) compared to DMSO controls. Results are shown as mean ± S.D. of three independent experiments. **P-value <0.01, ***P-value <0.001.
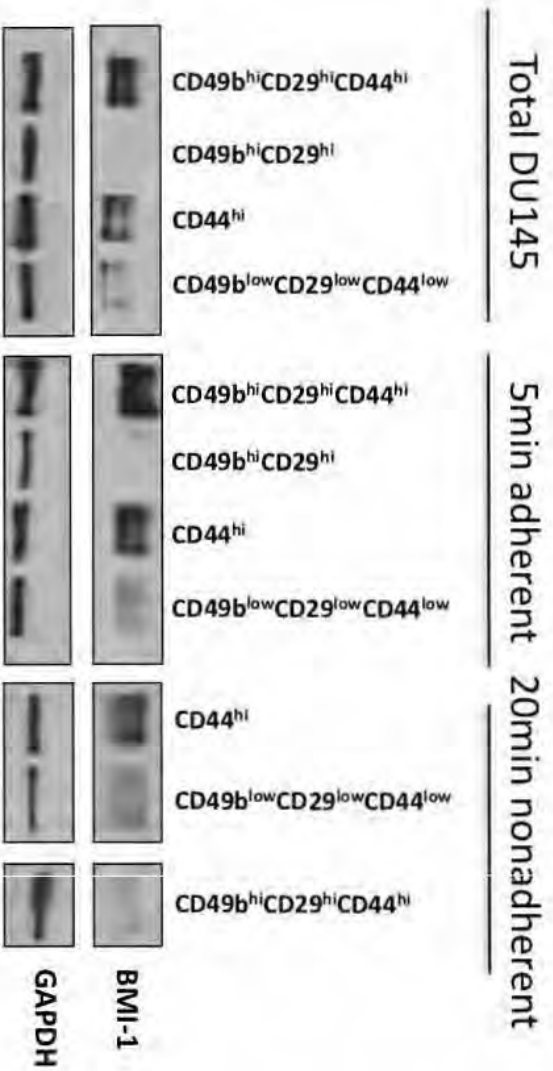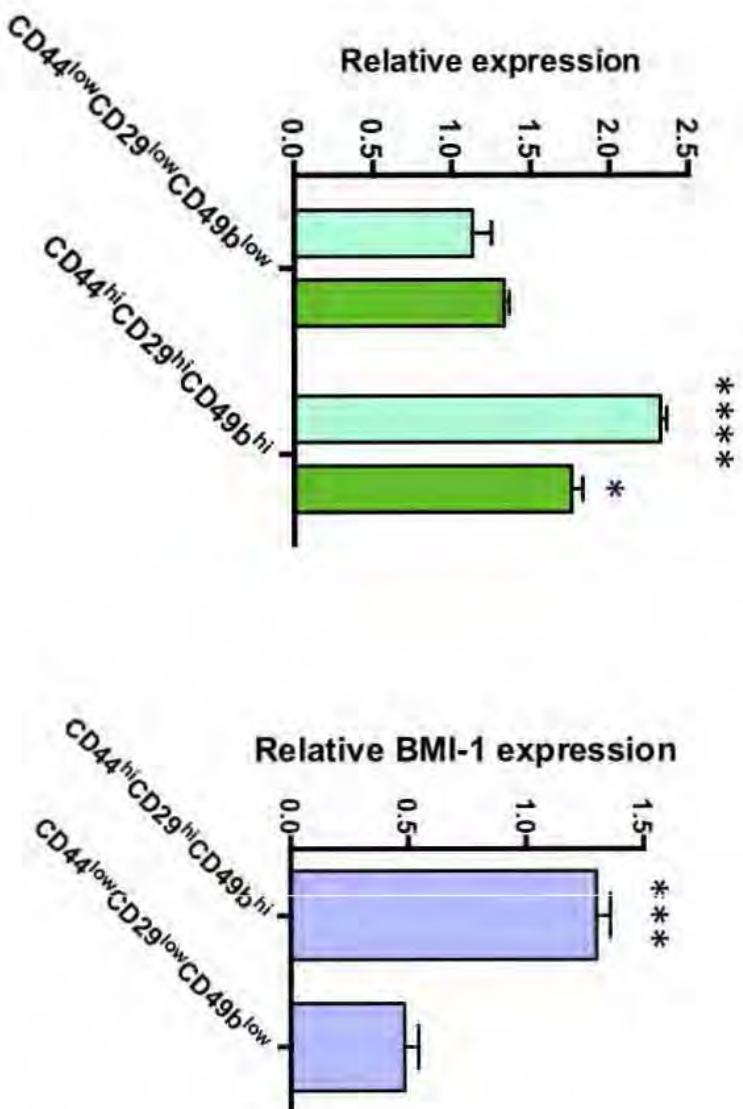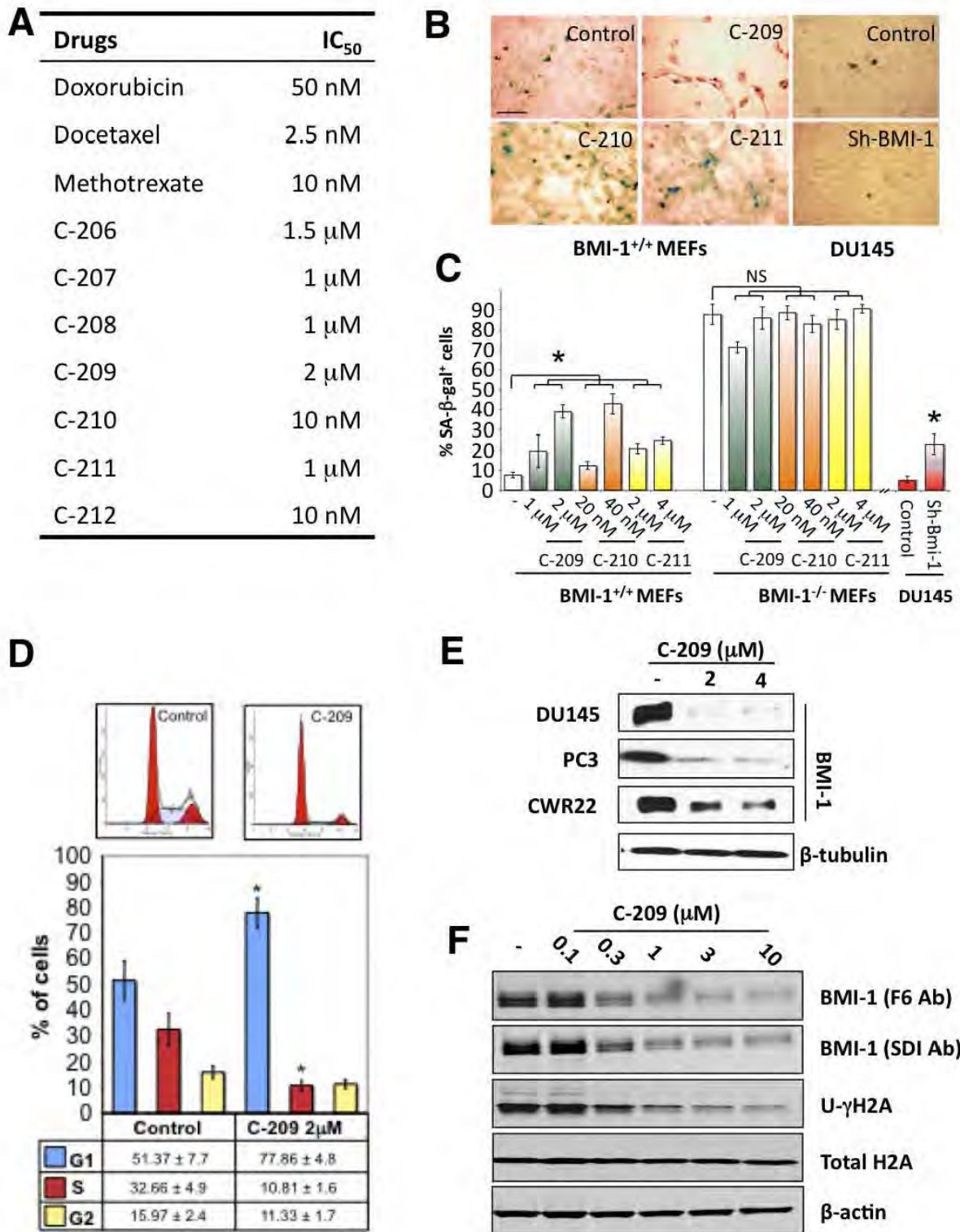
Supplementary Figure S2 BMI-1 expression in subpopulations of DU145 cells. **(A)** Western blot analysis for BMI-1 expression in subpopulations of adherent, nonadherent and/or sorted DU145 cells. GAPDH was used for equal loading. **(B)** Q-PCR analyses of CD49f (integrin-α6) and TROP2 in subpopulations of DU145 cells. **(C)** Q-PCR analyses of BMI-

2

1 in subpopulations of DU145 cells. Comparison of the differences in relative expression between each subpopulation and total CD49b^{low}CD29^{low}CD44^{low} DU145 cells was determined using Mann-Whitney U test. Graph indicates significant enrichment of CD49f (****$p<0.0001$) TROP2 (*$p<0.05$) in **b** and BMI-1 (***$p<0.001$) in **c**, in the 5min adherent CD49b^{hi}CD29^{hi}CD44^{hi} cells *vs.* CD49b^{low}CD29^{low}CD44^{low} DU145 cells. Results are shown as mean ± S.D. of 3 independent experiments.

A

Drugs	IC_{50}
Doxorubicin	50 nM
Docetaxel	2.5 nM
Methotrexate	10 nM
C-206	1.5 μM
C-207	1 μM
C-208	1 μM
C-209	2 μM
C-210	10 nM
C-211	1 μM
C-212	10 nM

Supplementary Figure S3 Pharmacological inhibition of BMI-1. (**A**) IC_{50} concentrations of doxorubicine, methotrexate, docetaxel and Bmi-1 inhibitors C-206 to C-212. IC_{50}s were determined using MTS assays on DU145 cells. (**B**) SA-β-gal staining of mouse embryonic fibroblasts (MEFs) and DU145 cells treated for 72h with C-209, C-210, or C-211 IC_{50}s. The reduced cell density in the image after treatment with C-209 is due to significant killing of DU145 cells. Scale bar is 50 μm. (**C**) Quantitation of SA-β-gal staining in control and C-209-, C-210-, or C-211-treated MEFS with (Bmi-1$^{+/+}$) or without Bmi-1 expression (Bmi-1$^{-/-}$), and in sh-Bmi-1 targeted DU145 cells. Note that Bmi-1-null MEFs have high levels

4

of senescence. (*p<0.01 compared to untreated cells, NS, not significant). (**D**) Cell cycle analyses assessed on DU145 cells treated with C-209 (2µM) for 72hrs. In bottom panel, results are shown as mean ± S.D. of three independent experiments (**E**) BMI-1 expression levels in DU145, PC3 and CWR22 PCa cells treated with increasing concentrations of C-209 (indicated). β-tubulin (shown only from DU145 cells) was used as loading control. (**F**) The expression of BMI-1 using two different antibodies (Targeting the full-length of the protein (F6 Ab) or the carboxyl terminal (SDI Ab)) in response to C-209. Notice the dose-dependent reduction of the C-terminal lysine-119 mono-ubiquitinated form of γ-H2A (U), a specific product of the BMI-1/PRC1 complex, compared to total H2A and β-actin.
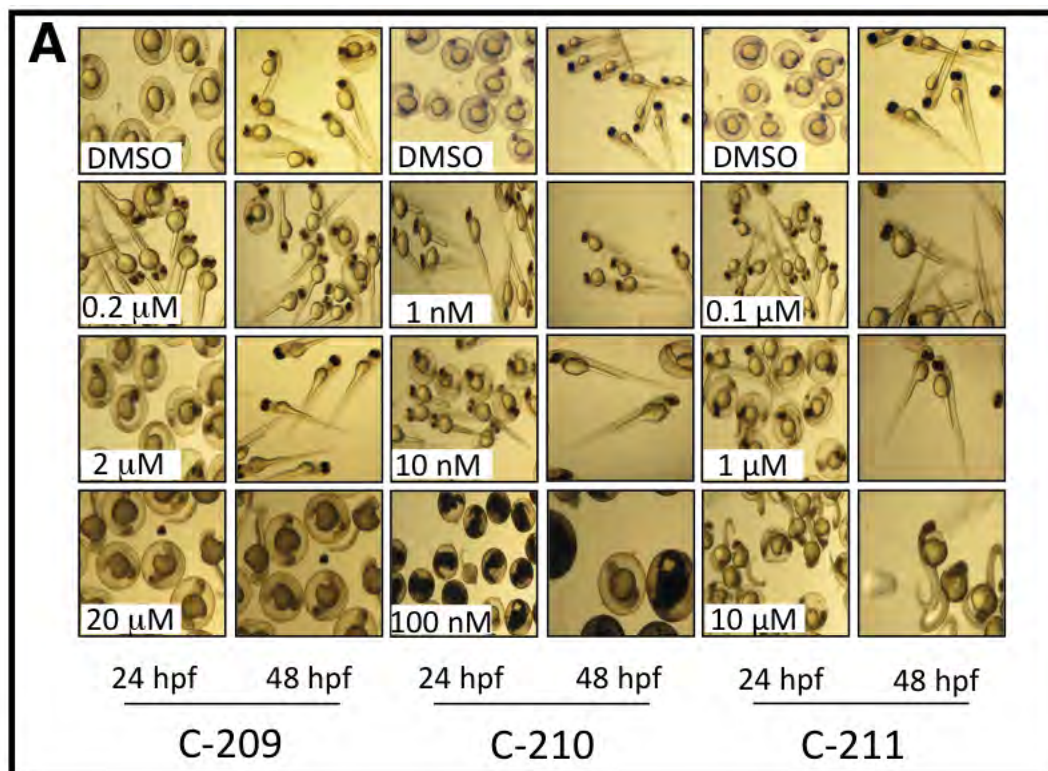
B Survival of zebrafish embryos after treatment with BMI-1 inhibitors (%)

	DMSO	C-209 (µM)			C-210 (nM)			C-211 (µM)		
		0.2	2	20	1	10	100	0.1	1	10
24 hpf	98 ± 1	97 ± 1	98 ± 1	90 ± 3	98 ± 1	96 ± 4	0	99 ± 1	98 ± 1	0
48 hpf	98 ± 1	98 ± 1	97 ± 2	65 ± 4	97 ± 1	90 ± 4	0	98 ± 1	98 ± 1	0

Supplementary Figure S4 Examining BMI-1 inhibitors in toxicological assays and effects on normal cells. (**A**) Bright field images of zebrafish embryos treated with BMI-1 inhibitors at the showed concentrations, and compared to vehicle treatment with DMSO. Progress in normal embryonic development is indicated by hatching of the embryos outside of the surrounding chorionic shell, typically occurring at 48-72 hour post-fertilization (hpf). The dark areas indicate necrotic tissues due to toxic effects. (**B**) Survival of zebrafish embryos after 24 and 48 hpf. In each treatment, at least 50 embryos were employed. Survivals are presented as mean percentage ± S.D. from three independent experiments. Compounds were dissolved in DMSO and added to embryo water starting at 12 hpf.

6

A

	0.5% DMSO	C-209 3μM	CHX 1μg/ml	CHX 5μg/ml	CHX 10μg/ml
1 dpf					
2 dpf					
3 dpf					
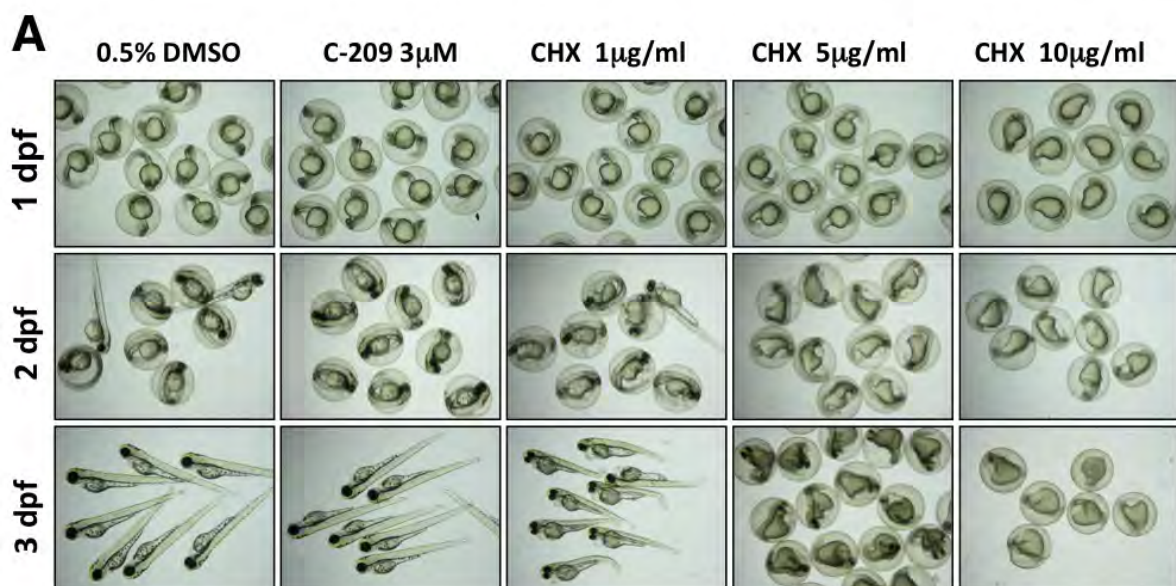
Survival of zebrafish embryos after treatments (%)

	DMSO	C-209 3μM	CHX 1μg/ml	CHX 5μg/ml	CHX 10μg/ml
24 hpf	98± 0.6	98± 0.6	98± 0.6	98± 0.6	98± 1
48 hpf	98± 0.6	98± 0.0	98± 0.6	0	0
72 hpf	98± 0.6	98± 0.0	97± 0.6	0	0

B

Survival of adult zebrafish after treatments (%)

	Controls	209 2μM	CHX 1μg/ml	CHX 5μg/ml	CHX 10μg/ml
24 hpt	100	100	100	0	0
48 hpt	100	100	100	0	0
72 hpt	93	100	90	0	0

Supplementary Figure S5 Toxicity effects of C-209 and CHX on adult and embryo zebrafish. (**A**) Upper panel: Bright field images of zebrafish embryos treated with Cycloheximide (CHX), C-209, or DMSO at the indicated concentrations. Compounds were added to embryo water at 12 hours post-fertilization (hpf) to examine the effects on embryo development and survival for 3 days. CHX treated embryos displayed toxic effects such as cardiac edema and curling of tails by 3dpf at the dose of 1 µg/ml. DMSO control and C-209 treated embryos appeared normal at 3dpf (days post-fertilization). At 5 µg /ml CHX, embryos appear mostly normal at 1dpf, but then die by 2dpf as determined by lack of a beating heart. At 10 µg/ml CHX, embryos demonstrate the developmental growth arrest sooner 18hpf to 1dpf, and are dead by 2dpf. At least 20 embryos were used per treatment. Lower panel: Survival table presented as mean percentage ± S.D. from three independent experiments. (**B**) Survival table of 6-10 week old zebrafish. A 12-well plate containing 4ml of treatment water and 2 fish per well was incubated at the normal fish maintenance temperature of 28.5 C for three days. Treatment water was changed daily due to accumulation of debris in the wells. The controls include untreated water, 0.5% DMSO, and 0.5% Ethanol. Ten fish per group were used in two independent experiments.
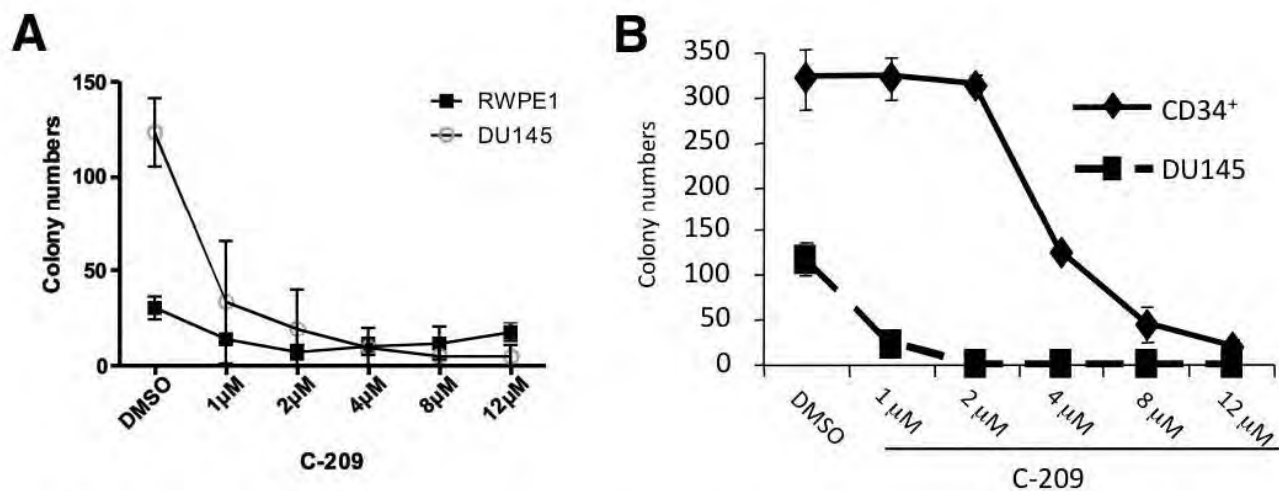
C Mice peripheral blood hematological profile following C-209 treatment

|	CTRL			C-209		
	Mean	±	SD	Mean	±	SD
WBC (x10³/μL)	1.22	±	0.92	1.34	±	0.53
Neutrophils	78.40	±	8.26	77.40	±	7.83
Lymphocytes	13.20	±	5.54	13.60	±	5.90
Monocytes	4.20	±	3.35	3.20	±	2.49
Eosinophils	3.60	±	4.34	5.20	±	4.38
Basophils	0.60	±	0.89	0.60	±	0.89
RBC (x10⁶/μL)	7.30	±	0.44	6.76	±	0.34
Hemoglobin	11.97	±	0.99	11.06	±	0.88
PLT (x10³/μL)	883.33	±	472.35	1442.20	±	136.92
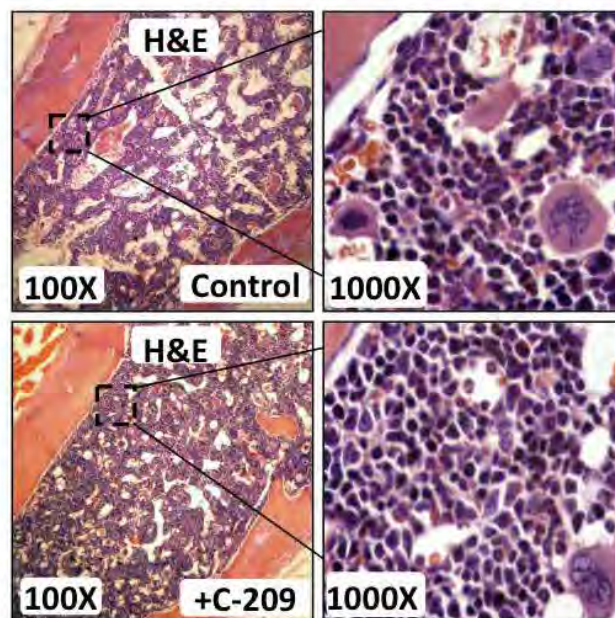
Supplementary Figure S6 BMI-1 inhibition effect on the normal prostate and hematopoietic system. (**A**) Normal epithelial RWPE1 and tumoral DU145 prostate cells were treated with the indicated concentration of C-209 for 72h. Subsequently, cells were collected, counted and 200 cells for each condition were plated to assess colony-forming

efficiency. Data plotted represent four independent experiments (p<0.0001 between DMSO and 1-12 μM in DU145 cells, NS between DMSO and 1-12 μM in RWPE1 cells). (**B**) Human CD34+ cells grown in methocult for hematopoietic colony assays and 200 DU145 cells were plated in 6-well tissue culture dishes and treated in parallel with C-209 at the indicated concentrations. Colony counts represent three independent experiments (p<0.0001 at 1-4 μM). **C**, Upper panel: Peripheral blood parameters of C-209-untreated and -treated mice (C-209 60mg/kg/day for ~2 weeks). All mice survived treatments with no apparent phenotypic changes. Peripheral blood was obtained from cardiac puncture bleeding and analyzed within 4hrs from mice sacrifice. N=9 mice/group were analyzed. Student's t-test comparing CRTL and C-209 treated mice indicates no significant differences between the two groups. Lower panel: hematoxylin/eosin staining of bone marrow biopsy sections from the femur derived at day 14 from the treated and untreated (Control) mice. Notice the similar cellularity of the bone marrow of the treated and control mice. The smears demonstrated the presence of heterogeneous cell types including the larger megakaryocytic lineages. Representative images were taken with 10× and 100x objectives.
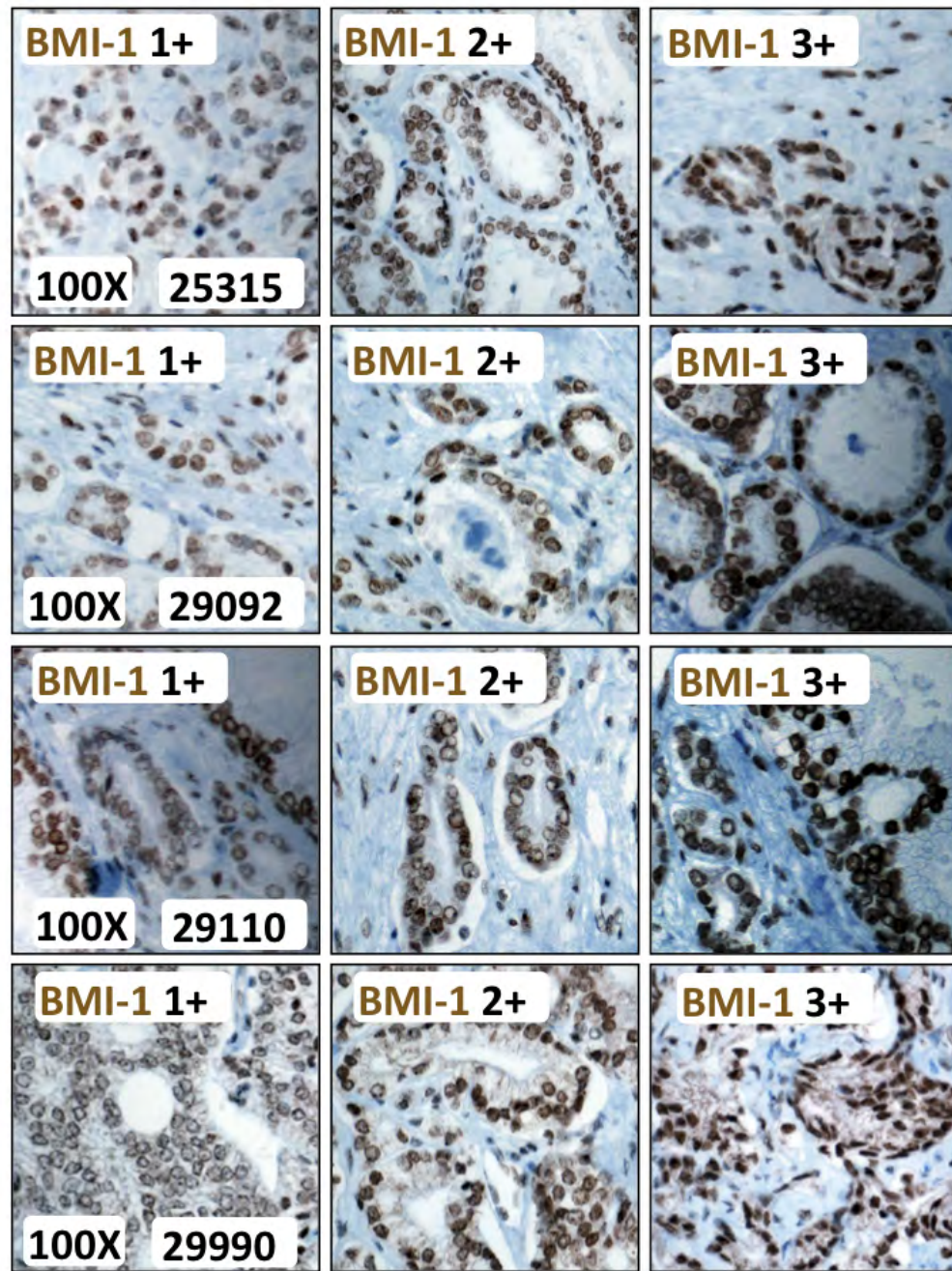
Supplementary Figure S7 Representative images of BMI-1 expression in primary PCa samples. BMI-1 expression was assessed as the extent of nuclear immunoreactivity by IHC. Score values for BMI-1 levels were: number of BMI-1 strongly staining nuclei (3+), number of BMI-1 moderately staining nuclei (2+), and number of BMI-1 weakly staining nuclei (1+). For each of the 4 representative patient derived tissues, heterogeneity of BMI-1 expression was observed.
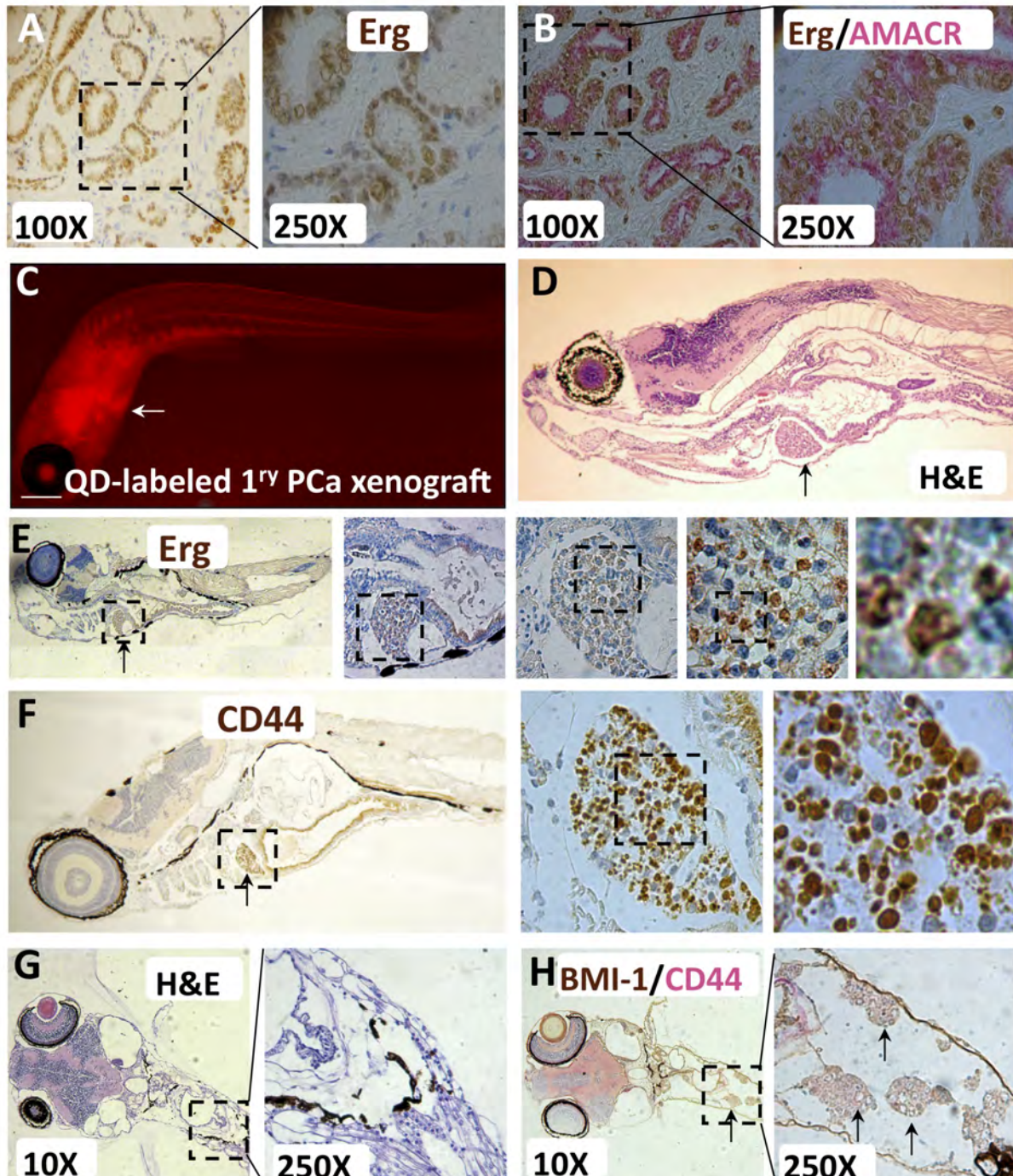
Supplementary Figure S8 Xenografts of primary PCa tissue in zebrafish embryos. (**A**) Section from primary PCa tissue identified to harbor the TEMPRESS-Erg fusion by FISH (not shown) demonstrates overexpression of Erg (brown) by IHC. (**B**) Co-localization of Erg (brown) and AMACR (pink) in PCa glands demonstrated by dual IHC staining. (**C**) Representative embryos transplanted with quantum-dot (QD) labeled primary PCa cells showing tumor formation as measured by red fluorescence at the 605 QD filter. (**D**) Histological sections from a representative zebrafish embryo at 8 days post-transplantation (dpt). (**E**) IHC demonstrating expression of Erg in the tumor graft cells (arrow in with higher magnifications in the right panels). (**F**) A representative zebrafish embryo at 12 dpt of the mirrorimages of primary cells in a demonstrating expression of CD44 in the tumor graft cells (arrow in with higher magnifications in the right panels). (**G-H**) Co-expression of CD44 and BMI-1 in the tumor graft cells (outlined areas in **G** and arrows in **H**). Scale bars are 250 µm in **C**, **D**, **F**, and 100 µm in **E** and **G-H**.

A

B
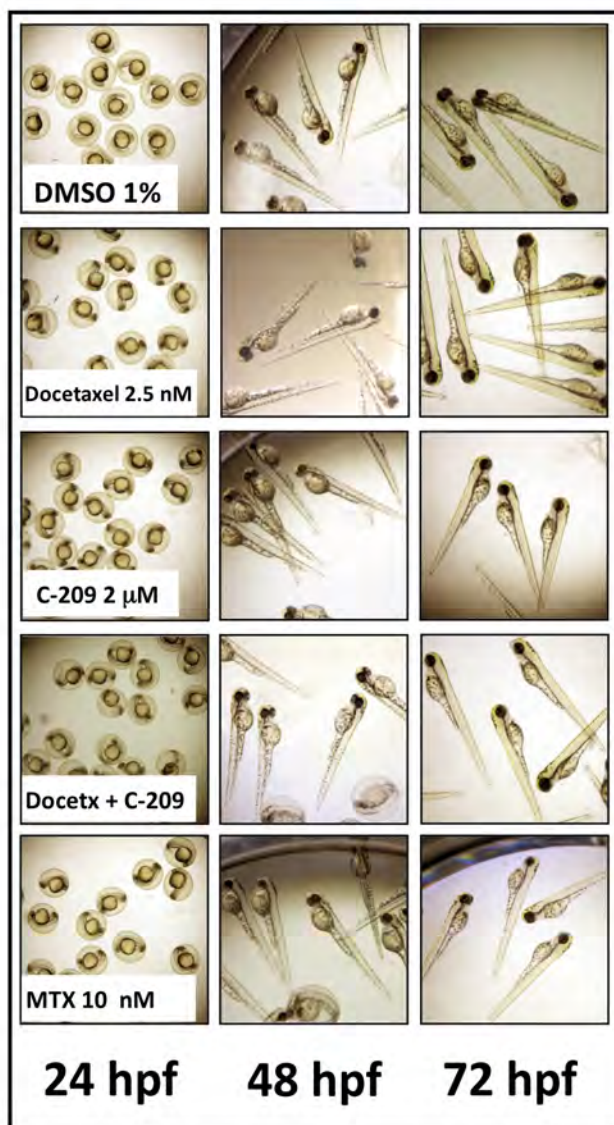
Survival of zebrafish embryos after treatments (%)

	1% DMSO	MTX	Docetaxel	C-209 2μM	Docetx+ C-209
24 hpf	100	100	100	100	100
48 hpf	100	100	100	100	100
72 hpf	100	100	100	100	100

Supplementary Figure S9 Toxicology assays of chemotherapy and BMI-1 inhibitors in embryonic zebrafish. (**A**) Bright field images of zebrafish embryos treated with chemotherapy and BMI-1 inhibitors at IC_{50} concentrations, and compared to vehicle treatment with DMSO. Compounds were added to embryo water after 6 hours post-fertilization (hpf) to examine the effects of these compounds on embryos that will be harboring tumor xenografts upon transplantation at 48-72 hpf and establish background fluorescence for treated embryos in the absence of human tumor cells. Treatment compounds, when used at IC_{50} concentrations had no notable toxic effects. At least 20 embryos were used in each treatment. (**B**) Survival of fish embryos upon treatment with C-209 and chemotherapy. Data are from two independent experiments utilizing 200 embryos per group.
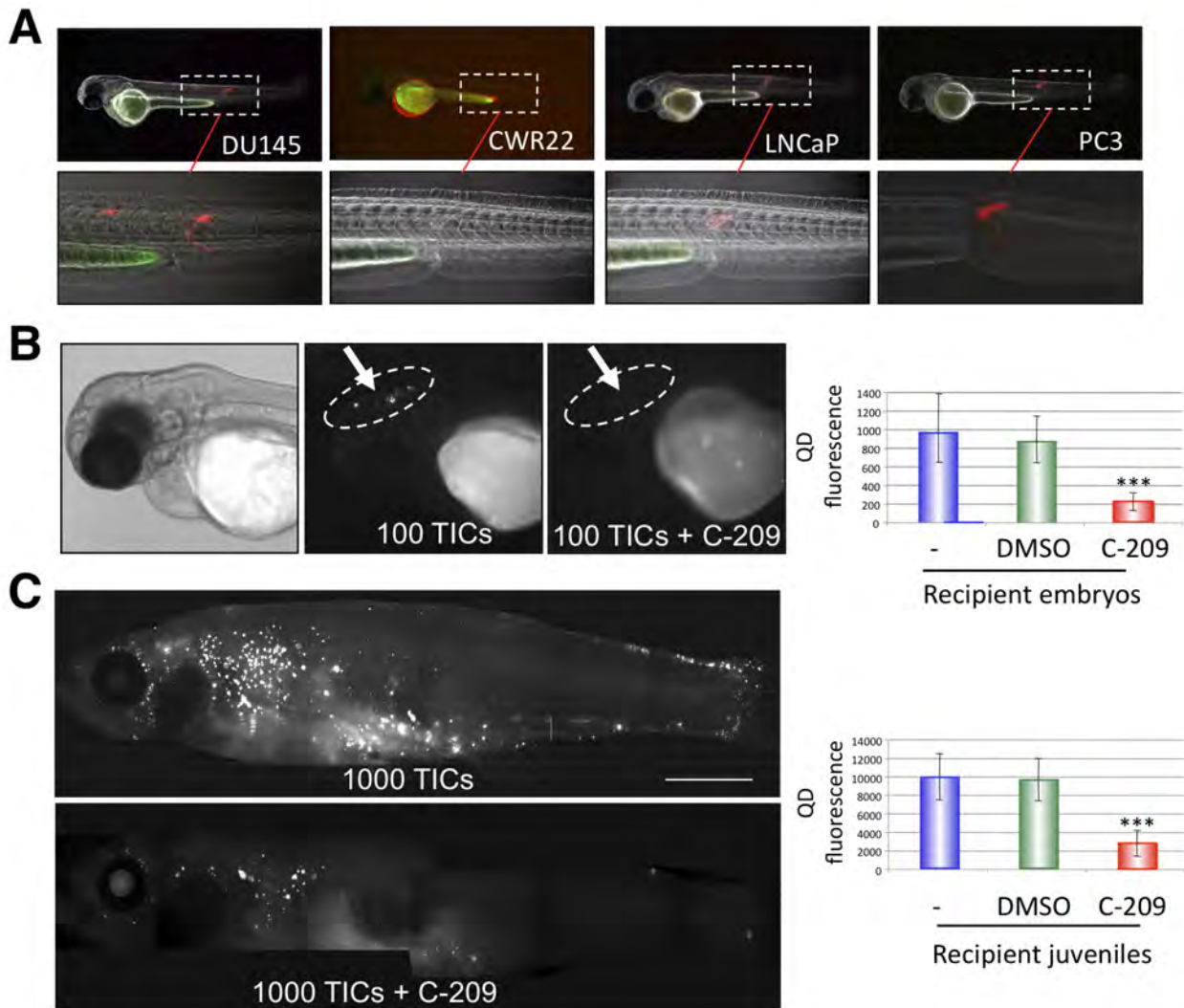
Supplementary Figure S10 Anti-tumor activity of BMI-1 inhibitors. (**A**) Representative images of embryos transplanted SC in the tail region with Q-dots-labeled rapidly adherent CD49b^{hi}CD29^{hi}CD44^{hi} (TICs) CWR22, LNCap, PC3, DU145 cells. Non-tumorigenic normal prostate cells were used as control and yielded no tumor formation. Images are overlays of bright field, GFP and red 605 fluorescent images from embryos that developed localized tumors with images taken during tumor development at 4 dpt. (**B**) Transplantation of 10 TICs resulted in brain metastasis in zebrafish embryos (arrow in outlined area). Exposure of the same embryo to the BMI-1 inhibitor C-209 at 2 µM in the water for 72 hours reduces the size and fluorescence emitted by DU145 cells growing in zebrafish embryonic brain (compare circled areas before and after treatment). Bright field image of this treated embryo is corresponding to the fluorescent image after treatment. Right graph demonstrates the QD fluorescence emitted by the tumor masses in outlined tumor regions of either untreated, vehicle, or C-209 treated embryos that were measured and displayed in arbitrary fluorescence units reflecting tumor growth or regression after treatment for 72 hours. Data represent 8 independent experiments displayed as mean ± s.d. derived from three replicate experiments using ≥20 embryo/group (*p<0.001). (**C**) Florescent composite images of whole juvenile zebrafish recipients transplanted with DU145 TICs. Images are lateral views with the head to the left. Transplantation of 500 TICs in conditioned juvenile zebrafish resulted in tumor growth, widespread migration, and metastasis of QD-labeled tumor cells throughout the fish. Treatment with C-209 at 2µM in conditioned water for 5 days reduced the size and fluorescence emitted by DU145 cells. The graph demonstrates QD fluorescence emitted by tumor masses in juvenile fish that are either untreated, vehicle or C-209 treated that were measured, and displayed in arbitrary fluorescence units reflecting tumor growth or regression. Data are displayed as mean ± S.D. derived from three experiments using 3 juvenile fish/group (*p<0.001).
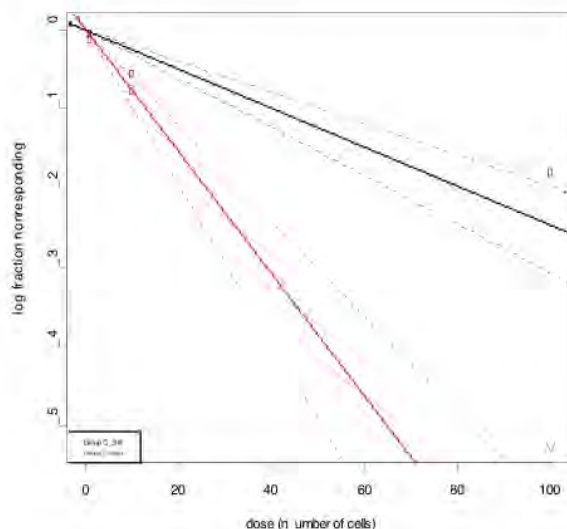
Confidence intervals for 1/(stem cell frequency)

	Lower	Estimate	Upper
Control	16.5	**12.9**	10.2
C-209	50.6	**40.6***	32.6

Differences in stem cell frequencies between the groups. *P value equals 4.9^{e-12}.

Number of cells plated	Colony Formation	
	Control	C-209
1	10/96	3/96
10	51/96	40/96
100	96/96	80/96

Supplementary Figure S11 Colony-formation frequency evaluated by dilution analysis of xenograft-derived cells from untreated mice and mice treated with C-209 60mg/kg/day. Data were analyzed using ELDA software (http://bioinf.wehi.edu.au/software/elda/). Upper panel: A log-fraction plot of the dilution model fitted to the data in the lower table. The slope of the line is the log-active cell fraction. The dotted lines give the 95% confidence interval. The data value with zero negative response at corresponding dose is represented by a down-pointing triangle.

Supplementary Methods

Western blot (WB) analyses

Pelleted cells were lysed and 50 µg of total proteins were separated on SDS PAGE gels and analyzed using: mouse monoclonal anti-BMI-1 clone F6 against the N-terminal (1:1000) (Millipore, rabbit polyclonal anti-BMI-1 SDI against the C-terminal (1:2,000) (SDI), mouse monoclonal anti-ubiquityl (γ)-histone H2A clone E6C5 (1:1,000) (Millipore), rabbit polyclonal anti-H2A (total) (1:1,000) (Millipore), anti-β-tubulin (1:5000) (Millipore), rabbit polyclonal anti-β-actin (1:10,000) (Rockland) and rabbit polyclonal anti-vinculin (1:1000) (Cell Signaling).

Genetic modulation of BMI-1 expression

For BMI-1 knockdown, DU145 cells were transfected with GIPZ Bmi-1 shRNA construct (Open Biosystems) using lipofectamine. Bmi-1 shRNA positive cells were selected in media with 0.5 mg/ml of puromycin. Selection was carried out in the presence of puromycin 5 µg/ml (Sigma). For BMI-1 overexpression, HEK 293T cells were transfected with pMcs-Bmi1-IRES-GFP retroviral vector along with packaging plasmids using the calcium phosphate method. The viral supernatant was used to infect DU145 cells, which were then selected through EGFP expression by cell sorting.

Migration assay

Cell migration was assessed in 24-well transwell boyden chambers (Costar Scientific Corporation, Cambridge, MA). PCa cells treated with docetaxel (2.5nM) and C-209 (2µM) for 96h were washed twice and replated in fresh medium without treatments for an additional 3 days. Consequently, $2x10^4$ cells/well were suspended in complete growth medium and placed into upper chambers. After 24 hrs, migrated cells were stained with Comassie Brilliant Blue and counted under the microscope.

Soft agar colony forming assays

To evaluate the fraction of self renewing cells, 500 cells were plated in the top agar layer in each well of a 24-well culture plate with 0.3% top agar layer and 0.4% bottom agar layer (SeaPlaque Agarose, Cambrex, NJ). Cultures were incubated at 37°C for 20 days. Colonies were stained after 3 weeks with crystal violet (0.01% in 10% MetOH), visualized and counted under microscope and photographed. For DU145 and RWPE colony formation assay, cells were treated with DMSO and C-209 (1μM, 2μM, 4μM, 8μM, 12μM). Colonies were enumerated over a period of 2 weeks. To perform clonogenic assay in soft agar *ex vivo*, DU145 Luc2EGFP xenograft-derived cells were isolated once tumors were aseptically removed and dissociated. Cells recovered were extensively washed and sorted for EGFP expression; next, 500 fluorescent cells for each treatment condition were plated as described above. After 20 days, colonies were visualized and counted.

Soft agar colony forming assays were carried out for primary PCa cells pre-treated with docetaxel (2.5nM) and C-209 (2μM) for 96h. Next, cells were collected, washed and replated in fresh medium in the absence of treatments for additional 3 days. Subsequently, cells were washed and 500 single cells were plated in the top agar layer in each well of a 24-well culture plate with 0.3% top agar layer and 0.4% bottom agar layer (SeaPlaque Agarose, Cambrex, NJ). Cultures were incubated at 37°C for 20 days. Colonies from triplicate wells were stained with crystal violet (0.01% in 10% MetOH), visualized and counted under microscope and photographed.

Cell viability assays

For chemosensibility studies, 5 x10^3 cells/well control vector-transduced (Sh-Scr) and BMI-1-depleted (shBMI-1) cells were plated in 96-well plates and treated with Docetaxel (2.5nM) or metotrexate (10nM) or the following concentrations of C-209: 0.0195, 0.0391, 0.0781, 0.1560, 0.3125, 0.6250, 1.25, 2.5, 5, 10, and 20 μM for 72hrs. Cell viability was always evaluated after 72hrs through MTS assay (Promega) following manufacturer's instructions. For primary cell survival assays, primary PCa cells were treated with docetaxel (2.5nM) or C-209 (2μM) for 4 days. Next, cells were collected, washed and replated in fresh media without treatments for an additional 3 days. On day 7, cells were collected and counted by Trypan Blue exclusion.

Cytotoxicity assays

Cytotoxicity of C-209, C-210, and C-211 compounds (PTC therapeutics) and methotrexate, doxorubicin and docetaxel were assayed following a 3-day exposure. DU145 Cells (3×10^3 cells/well) were treated with multiple concentrations to determine an IC_{50}, and toxicity analyzed using MTS assay (Sigma) per manufacturer's instructions. IC_{50} concentrations were determined using Hill's equation in Graph-Pad prism 4.0 software.

β-gal assay for senescence

Senescence experiments were performed in two 6-well plates for each treatment. Percentage of senescent cells was determined based on counts of 1,000 cells per treatment. Treatment with C-209 resulted in significant increase in senescence of DU145 cells that was detected with β-gal staining. Cells were fixed in 4% paraformaldehyde, washed in PBS pH 7.4 followed by PBS pH 6.0 for one hour each. Fixed cells were then stained with 2μg/ml x-gal (Sigma) overnight at 37°C and washed with PBS pH 6.0. Cells were imaged and staining was quantitated using Adobe Photoshop and ImageJ. The β-gal staining intensity was measured using the average intensity density of hue saturation.

In vitro prostasphere assay

Prostate tumor cell spheroid assay from cells lines was performed based on established methods [1-3], while we [4] and others [5-7] have previously described the spheroid assay from primary human prostate cancer cells. Prostate cells were counted and re-suspended at 2×10^3 cells/well in KSFM media and plated on 1% agarose coated plates. The cellular suspension was then plated in the well on 12-well plates and incubated at 37°C for 30 min. One milliliter of defined media was then added to each well and plates were replaced in 37°C incubator. For dissociation and passage of prostaspheres, incubation for one hour in 1 mg/ml Dispase (Invitrogen) was performed. Spheres were collected, washed in RPMI, and trypsinized (TripLE 200microliters/12-well plate). Every 3 days, half of the media was replaced and prostaspheres of >50 µm in diameter and consisting of >50

cells were counted on day14. Prostate cells obtained from dissociated primary prostaspheres remained viable after freeze/thaw, with formation of new prostaspheres that could be serially passaged. Dissociated prostaspheres could be passaged >3 generations. Single cells from day-7 prostaspheres were used in secondary and tertiary spheroid assays, and secondary or tertiary prostaspheres with size and morphological features similar to primary prostaspheres were counted.

Docking of C-209 to the human BMI-1 RNA

The interaction energy scores (E_{int}) are used to estimate the binding energy in the UCSF DOCK scoring of C-209 with BMI-1 RNA [8]. The docking was performed keeping the RNA structure rigid while permitting flexibility and full rotation and translation in the small molecule [8]. The imidazo-pyrimidine ring of C-209 mimics the purine ring of guanine, therefore, guanine was used as a reference. UCSF DOCK scores were E_{vdw} (kcal/mol), E_{elec} (kcal/mol), and E_{int} (kcal/mol), were generated using the following equation: $E_{int} = E_{vdw} + E_{elec}$. The lower the interaction energy score; the more stable the complex contacts with the RNA due to complete fitting into the binding pocket. C-209 UCSF DOCK scores were E_{vdw} (kcal/mol) -60.6, E_{elec} (kcal/mol) -5.2, and E_{int} (kcal/mol) -65.8, as compared to guanine scores of E_{vdw} (kcal/mol) -36.4, E_{elec} (kcal/mol) -4.1, and E_{int} (kcal/mol) -40.5, respectively, when $E_{int} = E_{vdw} + E_{elec}$. The lower the interaction energy score; the more stable the complex [9]. Therefore, C-209 is predicted to form the most stable complex with BMI-1 RNA. Guanine has a higher E_{vdw} energy owing to its inability to have more van der Waals contacts with the RNA due to its smaller and less complete fitting into the binding pocket.

Flow cytometric analysis

Cells were treated with C-209 2μM. After 72hrs, treated and untreated cells were stained with a propidium iodide (PI) staining solution (trisodium citrate 0.1%, NaCl 9.65μM, NP40 0.3%, PI 50μg/ml and RNase A 200μg/ml) for 30 min at RT. Cell cycle profile was acquired with a BD FACSCalibur flow cytometer (Becton Dickinson) and analyzed with FlowJo software (Tree Star Inc.; http://www.flowjo.com/index.php).

Cell sorting

For cytofluorimetric analyses, PCa cells were washed in 1xPBS, 2% FBS and 0.01% sodium azide and stained with isotype controls or anti-CD44-APC (Miltenyi) and anti-CD49b/CD29-FITC (BD). Cells were also stained with 7AAD to exclude dead cells. The effects of C-209 (2µM) on CD44 and CD49b/CD29 expression were assayed in DU145, PC3 and CWR22 and patient-derived cells (Patients # 28869, 33020, 33120, 33072, and 33106) after 72hrs of treatment. Acquisitions were made using a BD FACSCalibur flow cytometer (Becton Dickinson, Franklin Lakes, NJ) and analysed using cell quest software. Cell sorting was performed on cells stained with CD44-APC or CD49b/CD29-FITC and sorted using Influx High Speed Cell Sorter (BD Biosciences). Sorted cells were washed with PBS and treated as needed for the different experiments.

CD34$^+$ and DU145 colony forming assay

CD34$^+$ cells were isolated from cord blood samples (Elie Katz umbilical cord blood banking center, NJ) using MACS magnetic column separation system (Miltenyi). Briefly, cells were magnetically labeled with CD34$^+$ microbeads, and run twice through magnetic columns to increase purity. Cell viability and purity were assessed by flow cytometry. Purified CD34$^+$ cells were supplemented with IL-3, rhTPO (Kirin brewery), and FLT3-L (Peprotech) cytokines. Cells were suspended at 3 x 10^3 concentration in one ml of methocult (Methocult GF H4434; Stem cell technologies). Both CD34$^+$ and DU145 cells were treated with DMSO and C-209 (1µM, 2µM, 4µM, 8µM, 12µM). Colonies were enumerated over a period of 2 weeks.

Microscopy and peripheral blood analyses

To evaluate bone marrow cellularity, histologic sections were stained with hematoxylin/eosin. For May-Grünwald-Giemsa staining, mice were sacrificed at the end of the treatment, femurs were harvested and marrow flushed with a 23G (0.45 × 10 mm) syringe needle to collect single-cell suspensions. Bone marrow sections and blood May-Grünwald-Giemsa–stained cells were analyzed with a Zeiss Axiostar Plus microscope equipped with an A-Plan 10× dry objective (numerical aperture: 0.25) and an A-Plan 100× oil objective (numerical aperture: 1.25), respectively (Zeiss). Images were taken with a Canon Power Shot G9 camera. Peripheral blood

was obtained from cardiac puncture bleeding of mice treated with either vehicle or C-209 60mg/kg/day for 2 weeks. Blood was dripped directly after removal into tubes containing 0.5 mol/L EDTA. Peripheral blood parameters were analyzed at a reference hematology laboratory (ANTECH Diagnostics) within 4 hours from bleeding.

Immunohistochemistry

For IHC, fixed paraffin-embedded tissue samples from human prostate tumors were stained with anti-BMI-1 antibody (Cell Signaling) following antigen retrieval. Sections were scored for percentage of positive cells as well as intensity on a 0-3 scale by pathologists blinded to treatment. Slides were analyzed with a Zeiss Axiostar Plus microscope equipped with an A-Plan 10× dry objective (numerical aperture: 0.25) and images were taken with a Canon Power Shot G9 camera.

Zebrafish Drug Treatments

The following compounds were diluted in egg water: C-209, Cycloheximide (CHX), Docetaxel, Methotrexate (MTX), DMSO, and Ethanol. For all treatments, fish were incubated at the normal maintenance temperature of 28.5°C for a 3-days toxicity test. Viable embryos staged at 12 hours post fertilization (hpf) were counted into 12-well plates; all egg water removed and 2mL of treatment water added. Bright field images were taken on 1dpf, 2dpf and 3dpf with a Canon Powershot digital camera adapted to a Zeiss Stemi 2000-C microscope. Six-week old zebrafish were placed in 4ml treatment water (drug diluted in fish system water) at 2 fish per well in a 12-well plate. For adults only treatment water was changed daily due to debris accumulation in the wells.

Transplantation of human prostate cancer cells in zebrafish

Cells were resuspended in 0.5x Dulbecco's PBS (DPBS) containing QD605 (red fluorescence) (QD605; Invitrogen) and lipofectamine at a ratio of 1:2 for 2 hours. Cells were suspended in 0.5x DPBS for transplantation into dechorionated and anesthetized (0.5x tricaine methanesulfonate, MS-222; Sigma) 48-hour

post fertilization (hpf) embryos using 15 μm (internal diameter) injection needles. Injections were either subcutaneously (SC), or above the yolk into the sinus venosus using a Celltram microinjector. After transplantation, embryos were incubated for 2 hours at 37°C, and were then maintained in a humidified incubator at 33°C. Human cells were monitored under fluorescent microscopy for homing and tissue repopulation.

Limiting dilution assay

Limiting dilution assays were performed on EGFP-sorted xenograft-derived cells. Briefly, xenografts from C-209 treated and untreated mice were removed and enzymatically dissociated. Recovered cells were extensively washed and sorted for EGFP in order to exclude any non human tumor cells; subsequently cells were plated at the density of ~1, 10, 100 and 1000 cells/well in 96-well plates under standard growth conditions. After 14 days, colonies were fixed and stained (20% methanol fixation followed by 0.1% crystal violet staining). Clonogenic capability was assessed visually under the microscope. Wells containing no colonies were excluded for the analysis. Tumor-formation frequency was evaluated by using Extreme Limiting Dilution Analysis (ELDA) software (http://bioinf.wehi.edu.au/software/elda/index.html).

Supplementary references

1   Essand M, Nilsson S, Carlsson J. Growth of prostatic cancer cells, DU 145, as multicellular spheroids and effects of estramustine. Anticancer Res 1993; **13** (5A):1261-1268.

2   Sgouros G, Yang WH, Enmon R. Spheroids of prostate tumor cell lines. Methods Mol Med 2003; **81**:79-88.

3   Tokar EJ, Ancrile BB, Cunha GR, Webber MM. Stem/progenitor and intermediate cell types and the origin of human prostate cancer. Differentiation 2005; **73** (9-10):463-473.

4   Bansal N, Davis S, Tereshchenko I *et al.* Enrichment of human prostate cancer cells with tumor initiating properties in mouse and zebrafish xenografts by differential adhesion. Prostate 2014; **74** (2):187-200.

5   Goldstein AS, Lawson DA, Cheng D *et al.* Trop2 identifies a subpopulation of murine and human prostate basal cells with stem cell characteristics. Proc Natl Acad Sci U S A 2008; **105** (52):20882-20887.

6   Garraway IP, Sun W, Tran CP *et al.* Human prostate sphere-forming cells represent a subset of basal epithelial cells capable of glandular regeneration in vivo. Prostate 2010; **70** (5):491-501.

7   Guo C, Zhang B, Garraway IP. Isolation and characterization of human prostate stem/progenitor cells. Methods Mol Biol 2012; **879**:315-326.

8   Shoichet BK, McGovern SL, Wei B, Irwin JJ. Lead discovery using molecular docking. Curr Opin Chem Biol 2002; **6** (4):439-446.

9   Pettersen EF, Goddard TD, Huang CC *et al.* UCSF Chimera--a visualization system for exploratory research and analysis. J Comput Chem 2004; **25** (13):1605-1612.